# Activity Dependent Regulation of Inhibitory Circuitry

**Activity-dependent regulation of inhibitory circuitry**

A dissertation presented

by

Nikhil Sharma

to

The Division of Medical Sciences

in partial fulfillment of the requirements
for the degree of
Doctor of Philosophy
in the subject of
Neuroscience

Harvard University
Cambridge, Massachusetts
July 2015

Dissertation Advisor: Dr. Michael E. Greenberg Nikhil Sharma

**Activity-dependent regulation of inhibitory circuitry**

**Abstract**

Inhibition controls information flow through a neural circuit by modulating synaptic integration, restricting action potentials, and coordinating the activity of ensembles of neurons. These functions are mediated by a diverse array of inhibitory neuron subtypes that synapse on defined domains of a postsynaptic neuron. Activity-dependent transcription controls inhibitory synapse number and function, but how this transcription program affects the inhibitory inputs that form on distinct domains of a neuron remains unclear. We find that behaviorally-driven expression of the transcription factor NPAS4 orchestrates the redistribution of inhibitory synapses made onto a pyramidal neuron, simultaneously promoting inhibitory synapse formation onto the cell body while destabilizing inhibitory synapses formed on the dendrites. This rearrangement of inhibition across a neuron is mediated in part by the NPAS4 target gene brain derived neurotrophic factor (BDNF), which specifically regulates somatic inhibition. These findings suggest that sensory stimuli, by inducing NPAS4 and its target genes, differentially control spatial features of neuronal inhibition in a way that restricts the output of the neuron while creating a dendritic environment that is permissive for plasticity.

**TABLE OF CONTENTS**

**List of Figures**

**Chapter 2**

**Acknowledgements**

There are many people who have been with me through the ups, downs, and challenges of the scientific process. Importantly, I would like to thank Mike for his everlasting support in all phases and aspects of being a scientist. I would like to thank Brenda for a fruitful collaboration studying the electrophysiological changes associated with neuronal activity. I would like to thank Aurel for collaborating on a detailed molecular characterization of Npas4. I would like to thank Florence for being immensely valuable to all aspects of the project. I would also like to thank past and present members of the lab and friends who helped in so many ways: Milena Andzelm, Bulent Ataman, Gabriella Boulting, Alissa Trepman, Heidi Browne, Lucas Cheadle, Tim Cherry, Sonia Cohen, Cameron Couch, Shela Durresi, Dan Ebert, Harrison Gabel, Caitlin Gilbert, Jesse Gray, Benyam Kinde, Emi Ling, Athar Malik, Caleigh Mandel-Brehm, Alan Mardinly, Seth Margolis, Kyle McElroy, Bumjin Namkoong , Liz Pollina, Will Renthal, Alan Rodrigues, Yanni Salogiannis, Amy Shyer, Mike Soskis, Ivo Spiegel, Hume Stroud, Susan Su, Mike Susman, Chris Tzeng, Tommy Vierbuchen, Jamie Webster, Lynn Yap and anyone else I simply have forgotten to mention. Last but not least, I would like to thank my mom, dad, and sister for being a foundation.

**Collaborator contributions**

**Chapter 1:** Written by Nikhil Sharma (N.S.) and Michael E. Greenberg (M.E.G.)

**Chapter 2:** N.S., Brenda Bloodgood (B.B.) and M.E.G. designed the experiments; N.S. and B.B. performed and analyzed the experiments

**Chapter 4:** Experimental procedures were designed by N.S. and B.B.

# Chapter 1: Introduction

**Experience and the nervous system**

Experience is encoded by patterns of neuronal activity which have the ability to modify properties of neuronal circuits. The modifications are thought to form the mechanistic basis of brain function. In a series of what is now regarded as classic experiments done by Hubel and Wiesel, they showed that occlusion of one eye during development disrupted the formation of ocular dominance columns (Hubel and Wiesel, 1963a; Hubel and Wiesel, 1963b; Wiesel and Hubel, 1963). These data were taken to suggest that experience and the development, maturation, and functional plasticity of the nervous system are inextricably linked. Over the next 60 years, hundreds of laboratories have expanded on these findings. Today, the findings of Hubel and Wiesel have been generalized well beyond the visual system to include neural circuits across the central nervous system. Although it is now widely appreciated that experience can modify the nervous system, there has been considerable debate about the mechanisms underlying this process. Several models have been proposed to explain this phenomenon but it is clear that this will be an area of active investigation for years to come.

One model of particular interest has been the hypothesis that evolving levels of neural circuit activity orchestrate plasticity in the developing and mature nervous system.

Evolving levels of neural circuit activity are commonly measured by numbers of action potentials fired by individual neurons. The action potential serves as the language by which the nervous system communicates and it can also initiate a variety of biochemical

and signaling cascades within active neurons resulting in the modification of synaptic strength and efficacy. A less explored phenomenon is that elevated levels of neuronal activity also result in rapid transcriptional changes and gene expression (Lonze and Ginty, 2002; West et al., 2002). Gene expression resulting from neuronal activity has been postulated to be a critical regulator synaptic plasticity as well as other aspects of neuronal function (Dash et al., 1990; Kandel, 2001).

**Synapse to nucleus signaling**

Activity-dependent gene transcription occurs when neurotransmitters such as glutamate engage glutamate receptors on neurons resulting in depolarization and subsequent firing of action potentials. The firing of action potentials then results in Ca2+ influx mediated in part through the L-type voltage-sensitive calcium channels (Greer and Greenberg, 2008). Voltage-gated Ca2+ channels have classically been appreciated to have a role in synaptic plasticity but have recently been intimately linked to biochemical signaling cascades that are capable of signaling to transcriptional machinery in the nucleus (Greer and Greenberg, 2008). These biochemical cascades link depolarization ultimately to activation of transcriptional cascades in the nucleus.

One major example of the immediate consequences of L-type Ca2+ channel signaling is the phosphorylation and activation of the transcription factor cyclic adenosine monophosphate response element binding protein (CREB). More specifically, activity-dependent phosphorylation of CREB at Ser133 allows for CREB to recruit the histone

acetylase CREB binding protein (CBP) which is required for recruitment of transcriptional machinery and subsequent initiation of activity-dependent transcription (Ginty et al., 1993). Notably, in a series of breakthrough studies using the mollusk *Aplysia*, which exhibit memory-like behaviors, showed a requirement of CREB activation in order to consolidate memories (Kandel, 2001; Montarolo et al., 1986). The regulation of learning and memory by CREB has also been demonstrated in several model systems in addition to Aplysia including rodent systems and drosophila (Waddell and Quinn, 2001). Despite these early studies implicating CREB in learning and memory the first wave of genetic evidence painted a much more complex and often contradictory picture.

The first genetic model of CREB function that was generated was a hypomorphic mutation in the *Creb* gene (Hummler et al., 1994). This complex mutation resulted in the removal of most isoforms of CREB; however, there is certainly some functional forms of CREB remaining resulting in some degree of remaining CREB-functionality (Blendy et al., 1996). Despite the limitations of this model system, this mutant established a methodology for testing models of activity-dependent transcription in learning and memory.

Initial studies with this mouse genetic model revealed impairments with spatial memory tasks and hippocampal LTP (Bourtchuladze et al., 1994). Due to the reported lethality of CREB loss of function (Lonze and Ginty, 2002; Lonze et al., 2002; Riccio et al., 1999),

mouse genetic tools expressing dominant negative CREB in a drug inducible manner have been generated (Kida et al., 2002). Experiments with these mouse showed similar deficits in learning and memory alongside hippocampal plasticity (Kida et al., 2002). Although using drug inducible systems represents a clear advance, one major obstacle faced by these studies was the general lack of spatial specificity endowed by mouse genetic tools. An additional complication arises when one considers the number of neurons that fire action potentials during a behavioral bout. In fact, in learning and memory paradigms, a rather small subset of neurons, sometimes no more than a 1-2% of the total neurons in a brain region, are firing action potentials, therefore, only a small subset of neurons in a given brain region would be engaging the activity-dependent transcription pathway. Therefore, it remained an open question as to whether brain-wide manipulation of CREB, which would affect both active and inactive populations of neurons, results in a generalized disruption of neuronal function.

In order to address cell-type or brain region specificity, in addition to mouse genetic tools, several investigators have made advances using microinjection of viruses encoding gain and loss of function forms of CREB. Josselyn and colleagues have demonstrated infusion of a virus carrying a dominant negative form of CREB into the amygdala impairs acquisition of fear memories (Han et al., 2007). It has also been observed that over expression of CREB in a similar system results in a hyper-activation of neurons and lowers the threshold for acquisition of fear memories (Kim et al., 2014). These results

are not restricted to fear memories as several groups have expanded these findings to other memory paradigms, notably those involving drugs of abuse. In an elegant set of experiments using viral and mouse genetic tools, it was suggested that removing neurons in the amygdala that engaged in activity-dependent transcription during the acquisition of fear memories was sufficient to 'erase' the fear memory (Han et al., 2009). These results together have been used to make the case for the necessity of activity-dependent transcription in learning and memory.

Although it is tempting to conclude that CREB mediated transcription, or activity-dependent transcription more generally, is essential for learning and memory, there still is considerable debate in the field as to whether CREB activation is a cause or merely a consequence of elevated activity levels in a neuron. There have been several reports suggesting that loss of CREB can be compensated for by family members (Gass et al., 1998; Kogan et al., 1997; Pittenger et al., 2002). Further complicating matters is the reported roles of CREB in a wide array of biological processes orthogonal to neuronal activity such as development and neuronal survival (Lonze and Ginty, 2002). Because of these reasons, it has remained a significant challenge to disambiguate the role of CREB in neuronal activity mediated processes from other well established roles of CREB.

**Mechanism of activity-dependent regulation of neuronal circuits**

Despite an abundance of studies implicating activity-dependent transcription in learning

and memory via CREB, major conceptual challenges have remained. One particular challenge revolves around the regulation of synaptic plasticity: how can activity-dependent transcription possibly achieve regulation of specific synapses? In particular, if synaptic activity results in a transcriptional response in the nucleus, information about which synapses have been activated will have been lost and therefore subsequent activity-dependent genes have no instructions as to which synapses were active and should subsequently be modified.

One attractive model to resolve this discrepancy was proposed by Frey and Morris in 1997 and termed the 'synaptic tagging' hypothesis. In this model, in response to neuronal activity, the specific synapses that are activated generate a temporary 'tag molecule' which is later used to retrieve activity-dependent mRNA and proteins to specifically modify the active synapse. One line of experimental support for this model was provided by Kandel and colleagues in which they show that although activity can mediate cell-wide increases in protein level, only active synapse 'capture' these protein products and allow them to cause subsequent modification of the synapse (Barco et al., 2002). However attractive this hypothesis may be, the identification of the molecular tag used by synapses has remained elusive and has yet to be determined, casting some doubt as to whether synaptic tagging is a sufficient explanation for how specific synapses may be modified by a transcriptional response.

**Activity-dependent regulation of inhibitory circuitry**

In addition, propagation of action potentials through neuronal circuits is also controlled by the balance between excitatory drive that depolarizes neurons and inhibitory drive that hyperpolarizes them. An emerging model suggests that the collective balance between excitation, inhibition, and gene transcription are important contributors to ultimate output of a neural circuit.

The number and strength of excitatory synapses have been shown to be modulated by activity and activity-dependent gene expression (Flavell et al., 2006; Malinow, 2003; Turrigiano et al., 1998). It has recently been reported that inhibitory synapses are broadly regulated by the activity-dependent transcription factor Npas4 *in vitro* (Lin et al., 2008). However, as is the case with activity-dependent transcription factors, it has yet to be demonstrated whether Npas4 regulates inhibition *in vivo*. Moreover, it is unknown if the Npas4-mediated gene program regulates all inhibitory synapses made onto a neuron, providing a gain control mechanism, or if it distinguishes among the large number of inhibitory synapses made onto a neuron. The focus of this proposal is to understand the circumstances under which activity-dependent gene expression is activated *in vivo* and how it subsequently shapes the processing of neurons within their resident circuitry.

The functional diversity of inhibitory synapses represents a major challenge in coupling activity-dependent gene expression to regulation of inhibition. For example, neurons

receive inhibitory synapses throughout their dendrites, soma, and axon initial segment that originate from diverse inhibitory neuron subtypes (Danglot et al., 2006; Freund and Buzsaki, 1996). Inhibitory synapses that impinge on the apical dendrites can modulate local integration of excitatory synaptic activity and prevent the generation of dendritic calcium spikes (Larkum et al., 1999; Miles and Poncer, 1996; Miles et al., 1996) while precisely timed somatic inhibition can prevent action potential generation or restrict the time window during which firing can occur (Glickfeld and Scanziani, 2006; Pouille and Scanziani, 2001). These functionally distinct types of inhibition are recruited in response to different levels of neural activity. This has been observed when inhibitory neurons that synapse on the dendrites or somata of pyramidal neurons are recruited or suppressed during different frequency oscillations (Buzsaki, 2002, 2005; Klausberger et al., 2003). Also, during trains of action potentials, inhibition of hippocampal pyramidal neurons has a somatic bias initially but as the train progresses, transitions to be more heavily dendritic (Pouille and Scanziani, 2004). Thus activity-dependent regulation of inhibitory synapses formed on distinct domains of the neuron will have significant consequences for the output of the pyramidal neuron and the evolution of how that neuron responds to ongoing circuit activity.

**Chapter 2: The activity-dependent transcription factor NPAS4 regulates domain-specific inhibition.**

**This chapter was modified from: *Nature*. 2013. 503:121-125.** 

**Background**

A diverse array of inhibitory neuron subtypes form synapses along the dendrites, soma, and axon initial segment of excitatory pyramidal neurons (Danglot et al., 2006; Freund and Buzsaki, 1996; Klausberger et al., 2005). Dendritic inhibition modulates integration of excitatory synaptic potentials and prevents the generation of dendritic calcium spikes (Chiu et al., 2013; Liu, 2004; Miles and Poncer, 1996; Miles et al., 1996; Turner and Schwartzkroin, 1983). Precisely timed somatic inhibition limits the number and time window during which action potential (AP) firing can occur (Atallah et al., 2012; Glickfeld et al., 2008; Glickfeld and Scanziani, 2006; Pouille and Scanziani, 2001, 2004). Several recent studies have shown that activation or suppression of inhibitory neurons that target the dendrites or soma of pyramidal neurons can alter the pyramidal neurons tuning properties and firing rates *in vivo* (Lee et al., 2012; Lovett-Barron et al., 2012; Pouille et al., 2009; Royer et al., 2010; Wilson et al., 2012). Thus, the regulation of the inhibitory synapses that form on distinct domains of a pyramidal neuron can have a profound effect on the output of the neuron and the evolution of how the neuron responds to ongoing circuit activity.

Despite the physiological importance of these processes, the molecular mechanisms that control somatic and dendritic inhibition remain to be identified. We investigated the possibility that NPAS4, an activity-regulated transcription factor that controls the number of inhibitory synapses that form on excitatory neurons in cell culture (Lin et al., 2008), might be a critical regulator of synaptic inhibition in vivo that is capable of differential

regulation of somatic and dendritic inhibition. To explore this possibility, we exposed mice to stimuli that trigger NPAS4 expression in the hippocampus and evaluated the effect of disrupting NPAS4 expression on somatic and dendritic inhibitory synapse function in acute hippocampal slices.

**Enhanced activity states induce NPAS4-dependent inhibitory synaptic plasticity**

In hippocampal CA1 pyramidal neurons from mice maintained in standard housing NPAS4 protein is undetectable by immunostaining (**Figure 1A**). By contrast, exposure of mice to an enriched environment (EE), consisting of a running wheel and novel objects to explore, induces NPAS4 expression in the nuclei of neurons in the pyramidal cell layer, while no NPAS4 positive nuclei are observed in the neuropil (**Figure 1B**). This indicates that the majority of neurons that express NPAS4 in response to environmental enrichment are excitatory, not inhibitory, neurons. To obtain more synchronous and widespread induction of NPAS4 in the hippocampus we injected mice intraperitoneally with kainic acid (KA), a glutamate analogue that induces seizure activity. This treatment led to NPAS4 expression in nearly all excitatory neurons in the pyramidal cell layer and a minority of inhibitory neurons with cell bodies located in the apical or basal neuropil (**Figure 1C**). Thus we conclude that most, if not all, hippocampal CA1 pyramidal neurons are capable of expressing NPAS4 protein and that exposure to an enriched environment or KA are viable strategies for inducing NPAS4 in vivo.

We next asked if the loss of NPAS4 affects inhibitory synapse function in vivo. At postnatal day 13-15 (P13-15), we injected adeno-associated virus expressing a Cre-GFP fusion protein (AAV-Cre-GFP) (Adesnik et al., 2008; Lu et al., 2009) into the CA1 region of the hippocampus in mice homozygous for floxed Npas4 alleles ($Npas4^{f/f}$). This strategy generated juvenile mice with unperturbed development and sparse, GFP+, Npas4 knock-out neurons surrounded by GFP-, Npas4 wild-type neurons, referred to as NPAS4-KO and NPAS4-WT neurons **(Figure 2)**,

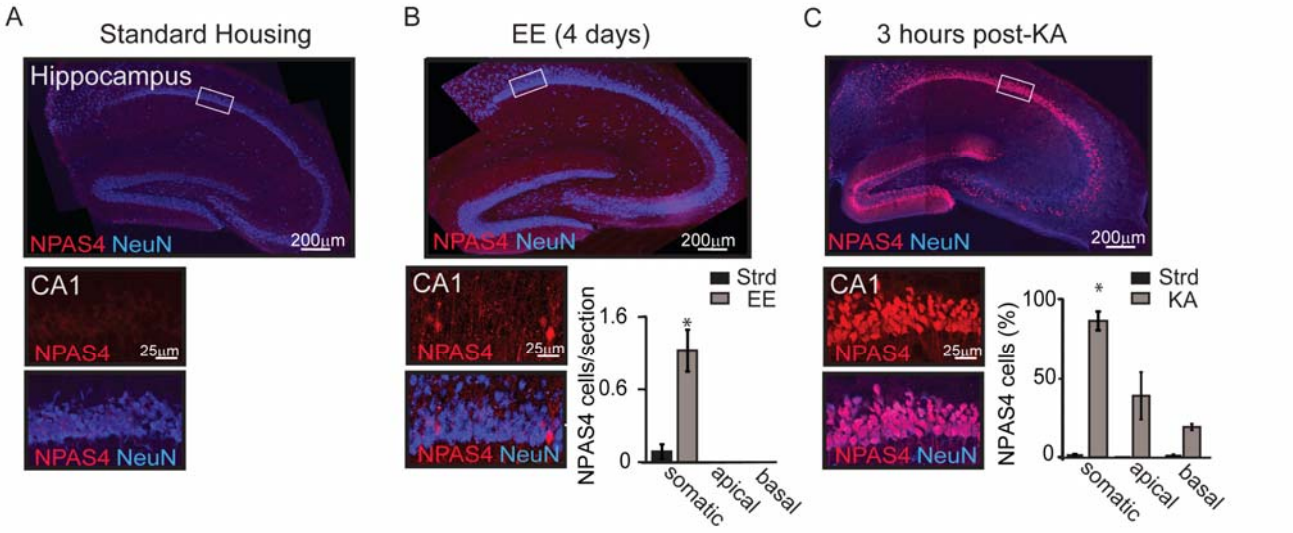


**Figure 1. Npas4 is regulated by neuronal activity *in vivo*.**

(A-C) Representative hippocampal section from a wild-type mouse housed in (A) standard laboratory conditions, (B) an enriched environment (EE) for 4 days, or (C) 3 hours post-kainic acid (KA) injection. Sections were immunostained for NPAS4 (red) and NeuN (blue) protein to highlight the pyramidal layer. Scale bar = 200µm. Higher magnifications of the boxed region are shown below. Scale bar = 25µm. Quantification of

**Figure 1 (Continued)**. NPAS4 expressing neurons are shown in (B, C). Data are shown as mean ± SEM. Significance was determined by two-tailed t-test. $p<0.01$.

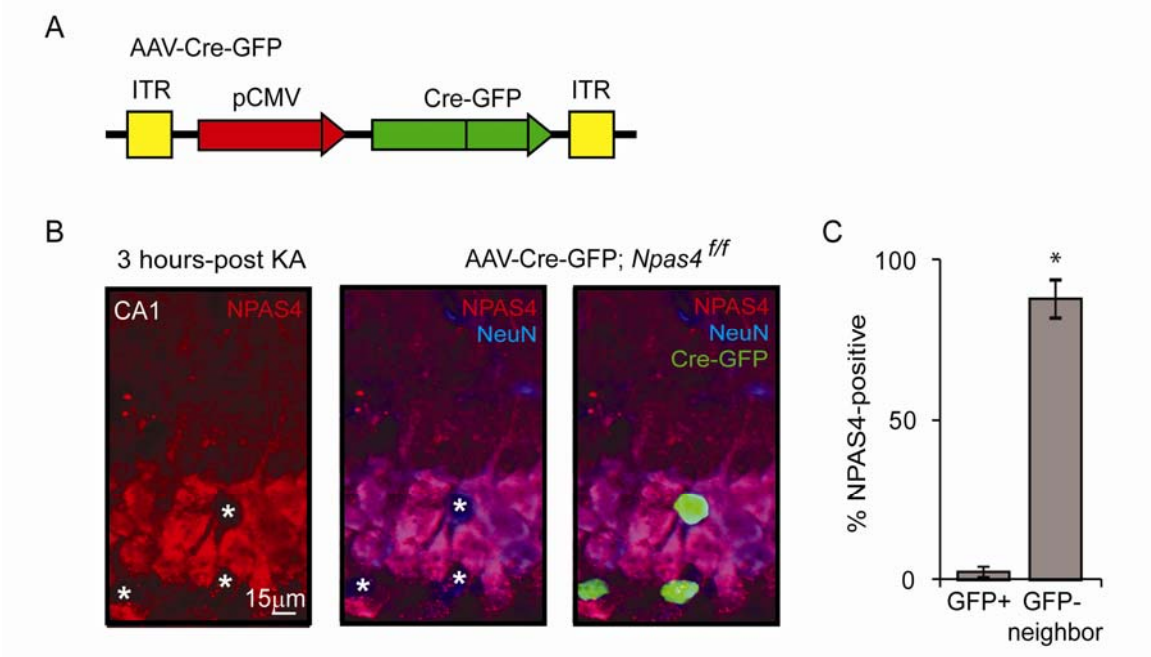


**Figure 2. Infection with AAV-Cre-GFP effectively excises Npas4**

(A) Schematic of the AAV-Cre-GFP virus genome.

(B) Representative hippocampal section from an AAV-Cre-GFP; Npas4f/f animal 3 hours post-KA injection. Sections were imaged for native GFP fluorescence (green) and immunostained NPAS4 (red) and NeuN (blue) protein.

(C) Quantification of neurons with overlapping GFP and NPAS4 in the sections represented in (B). Data are shown as mean ± SEM. $p < 0.01$ by two tailed t-test.

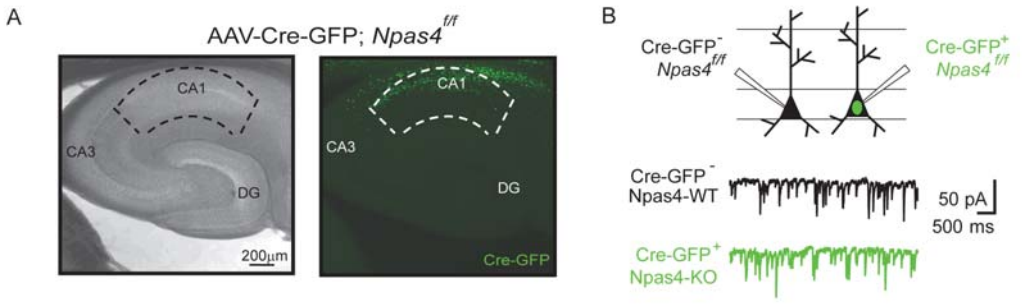


**Figure 3. Stereotaxic surgery can be used to target the CA1 region of hippocampus and allow for paired whole-cell recording configuration.**

(A) Wide field (left) and fluorescence (right) image of an acute hippocampal slice from an Npas4f/f mouse sterotaxically injected with AAV-Cre-GFP virus. Infected neurons are GFP+. Dashed line outlines the CA1 field of the hippocampus.

(B) Schematic of the experimental configuration. mIPSCs were measured from neighboring NPAS4-WT (Cre-GFP-, black) and NPAS4-KO (Cre-GFP+, green) neurons. Representative mIPSC recordings from NPAS4-WT (black) and NPAS4-KO (green) neurons.

respectively (**Figure 3**). This approach allowed us to assess the effects of acute NPAS4 loss while minimizing the number of presynaptic neurons that are NPAS4-KOs. Postoperatively animals were either transferred to an enriched environment or maintained in standard housing. Seven to twelve days post-injection, acute hippocampal slices were prepared, whole-cell voltage clamp recordings were made from neighboring NPAS4-KO and NPAS4-WT neurons and pharmacologically isolated miniature inhibitory postsynaptic currents (mIPSCs) recorded (**Figure 4**). By comparing neighboring NPAS4-KO and NPAS4-WT neurons we were able to precisely control for variability in local infection densities and differences in an individual animal's interaction with the environment.

We found that when mice were exposed to an enriched environment significantly less frequent and slightly smaller amplitude mIPSCs were recorded from NPAS4-KO neurons compared to the neighboring NPAS4-WT neurons (**Figure 4B, freq: $p<0.05$**). Similar results were obtained from mice injected with KA to induce NPAS4 (**Figure 4C , freq: $p<0.01$, amp: $p<0.05$**). By contrast, no significant difference in mIPSC frequency or amplitude was observed between neighboring wild type and NPAS-KO neurons in slices acquired from mice maintained in standard housing (**Figure 4A, Supplemental Table 1**). We also measured mIPSCs in comparably manipulated wild type mice and detected no change in mIPSC frequency or amplitude (**Figure 5**) indicating the observed changes in mIPSCs in $Npas4^{f/f}$ neurons infected with AAV-Cre-GFP are specifically due

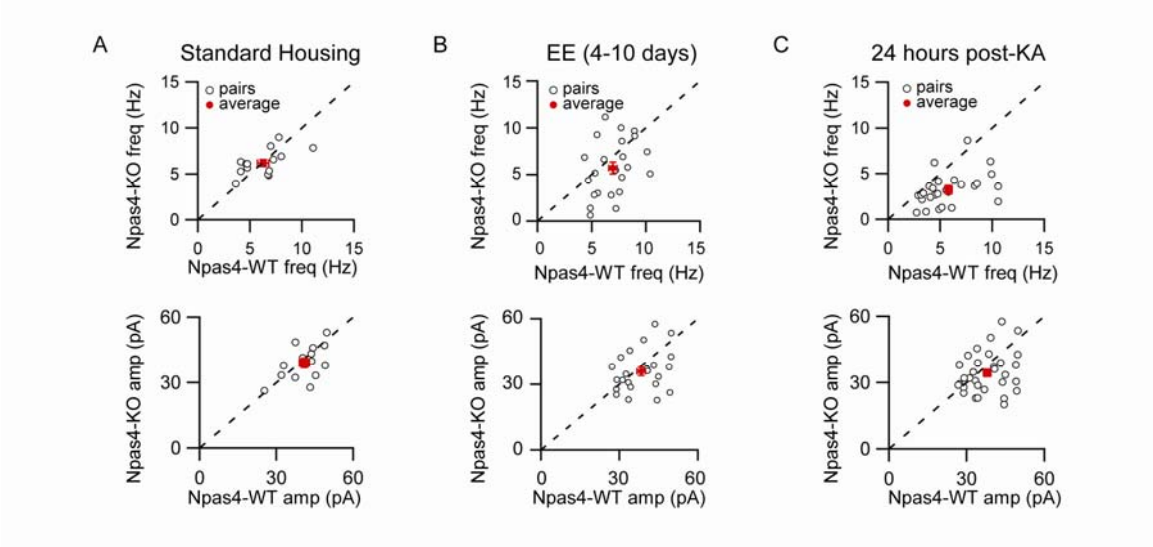


**Figure 4. Exposure of mice to elevated circuit activity reveals an NPAS4-dependent decrease in mIPSC frequency and amplitude in vivo.**

(A-C) mIPSC frequency (top) and amplitude (bottom) recorded from neighboring NPAS4-WT and NPAS4-KO neurons from mice maintained in (F) standard housing, (G) EE (4-10 days), or (H) 24 hours post-KA. Open circles indicate individual NPAS4-KO/NPAS4-WT pairs. Red circles indicate the mean ± SEM. Significance was determined by paired two-tailed t-test.

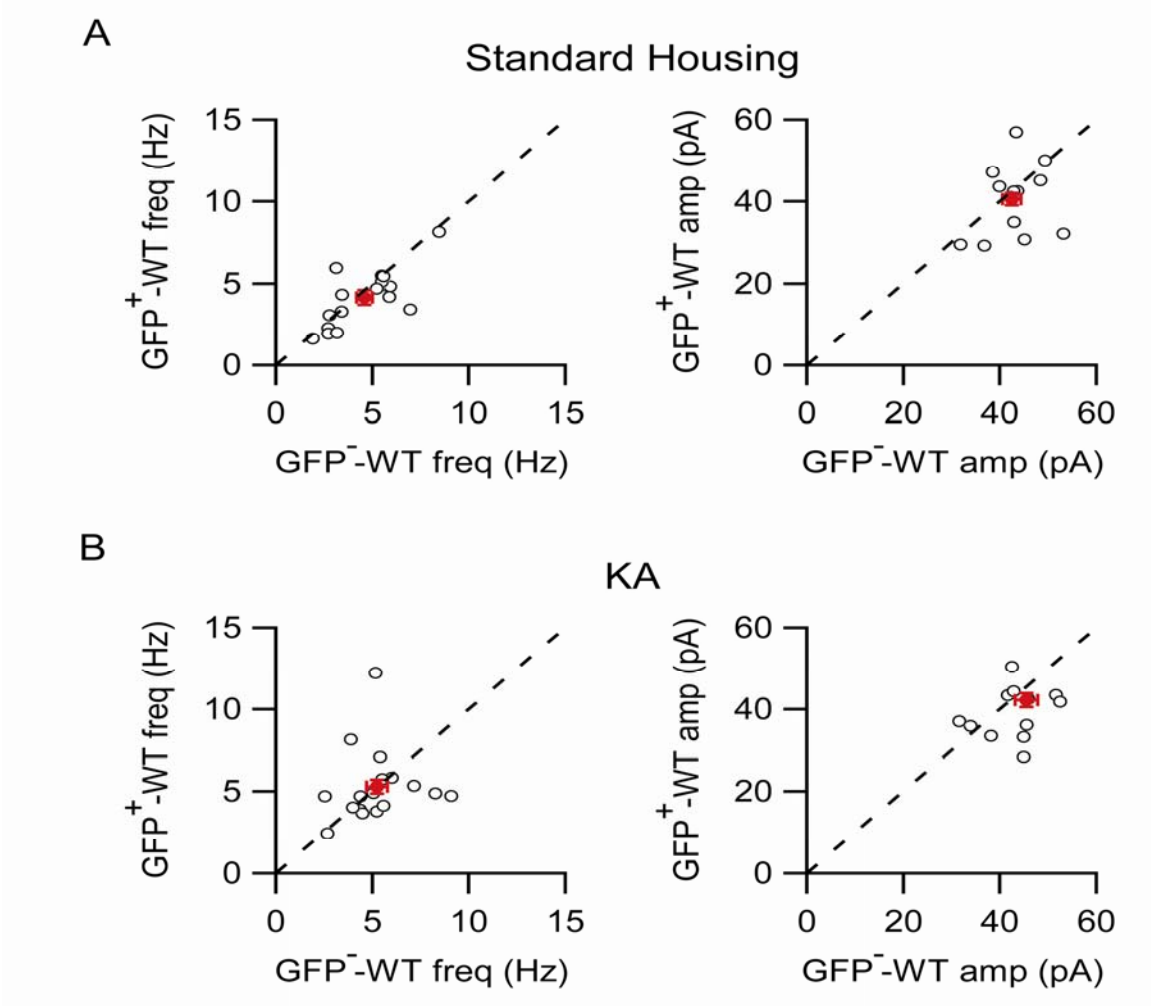


**Figure 5. AAV-Cre-GFP does not change mIPSCs in wild type mice.**

(A) mIPSCs frequency (left) and amplitude (right) were measured from pairs of neighboring GFP+ and GFP- neurons from wild-type (C57Bl/6) mice maintained in standard housing. Open circles indicate individual GFP+/GFP- pairs. Red circles indicate mean ± SEM.

(B) mIPSCs frequency (left) and amplitude (right) were measured from pairs of neighboring GFP+ and GFP- neurons from wild-type (C57Bl/6) mice 24 hours after

**Figure 5 (Continued)**. injection of KA. Open circles indicate individual GFP+/GFP- pairs. Red circles indicate mean ± SEM. Significance was determined by paired two-tailed t-test.

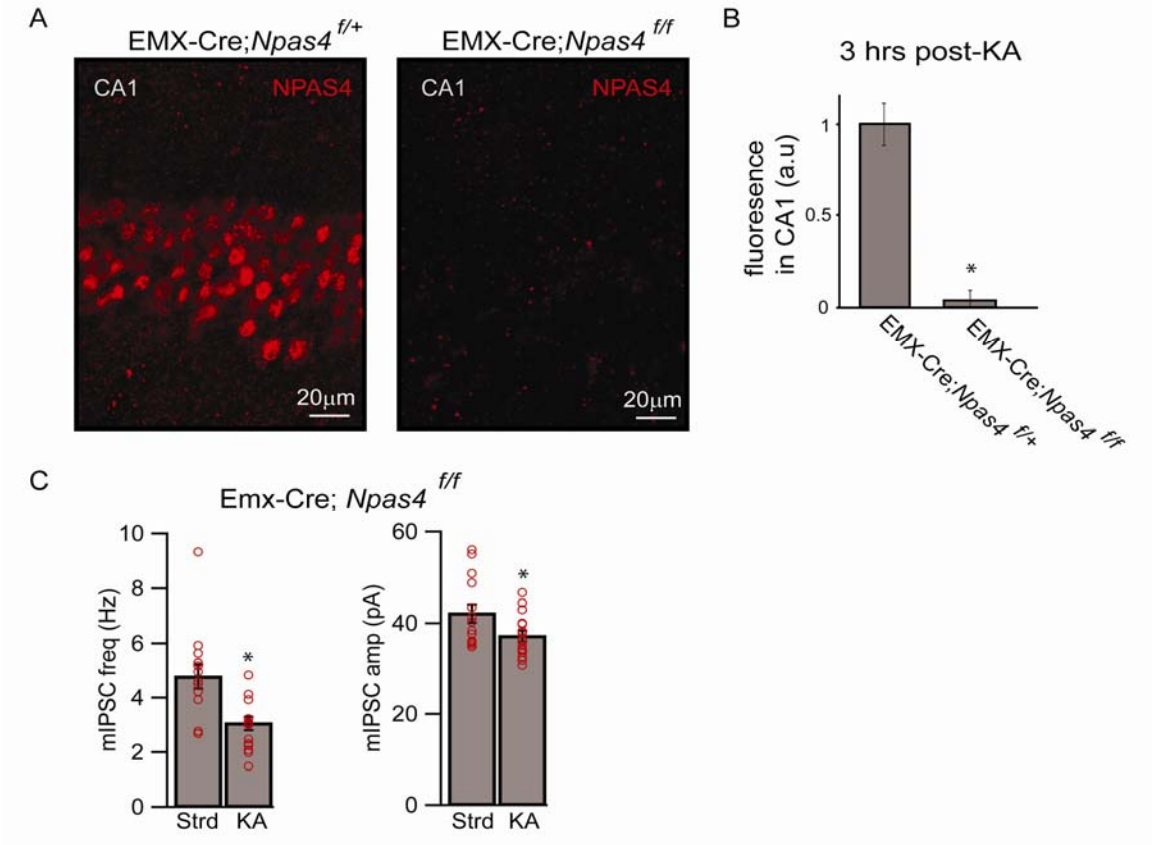


**Figure 6. Excision of NPAS4 specifically from excitatory neurons reveals an activity-dependent** decrease in mIPSC frequency and amplitude.

(A) Representative hippocampal CA1 section from an EMX-Cre;Npas4f/+ and EMX-Cre;Npas4f/f mouse 3 hours post-KA injection. Sections were immunostained for NPAS4 (red) protein.

(B) Quantification of NPAS4 immunoreactivity in the pyramidal layer of CA1. Data are shown as mean ± SEM.

(C) mIPSCs frequency and amplitude measured from neurons in EMX-Cre;Npas4f/f mice maintained in standard housing or 24 hours post-KA injection. Bars indicate mean ±

**Figure 6 (Continued)**. SEM. Red circles indicate individual neurons. Significance was determined by two-tailed t-test, *frequency: $p<0.01$, amplitude: $p<0.05$.

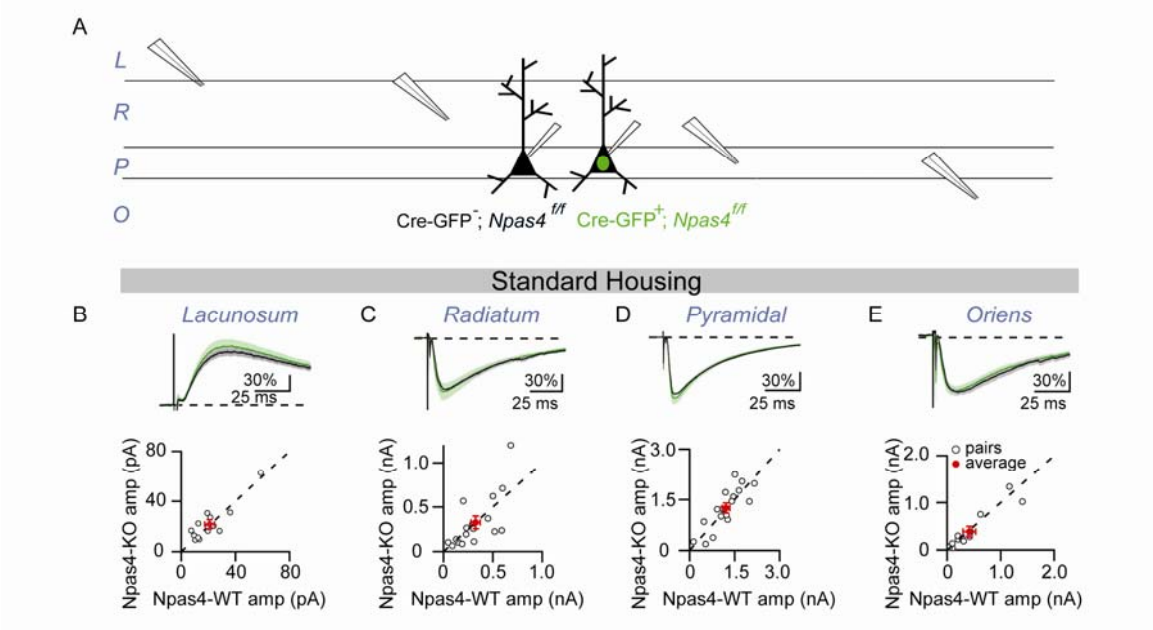


**Figure 7. Npas4 does not alter inhibitory synaptic transmission across the somatodendritic axis under standard housing conditions.**

(A) Schematic of experimental configuration. A stimulating electrode was placed in one of the four layers of CA1 and local axons depolarized. eIPSCs were measured simultaneously from neighboring NPAS4-WT (black) and NPAS4-KO (green) neurons. Layers - L: lacunosum-moleculare, R: radiatum, P: pyramidale, O: oriens.

(B-E) eIPSCs measured from mice maintained in standard housing. Top: Normalized, average eIPSC measured from NPAS4-WT (black) and NPAS4-KO (green) neurons in response to stimulation of axons in (B) lacunosum-molecular, (C) radiatum, (D) pyramidale, or (E) oriens are shown. Currents were normalized pairwise to the peak of the NPAS4-WT eIPSC. Data are shown as the mean (line) ± SEM (shaded region). Scale bars: 30% change in normalized current, 25 ms

to Npas4 excision in these neurons and not a consequence of viral infection or Cre expression. From this analysis we conclude that disruption of behaviorally induced NPAS4 expression leads to a decrease in mIPSC frequency recorded from CA1 hippocampal pyramidal neurons.

To determine if the observed changes in mIPSCs are due specifically to excision of Npas4 in excitatory neurons we crossed EMX-Cre and Npas4$^{f/f}$ mice to generate animals that lack NPAS4 postnatally and in all excitatory neurons but have unperturbed NPAS4 expression in inhibitory neurons (**Figure 6**). To maximize NPAS4 induction in these experiments mice were injected with KA. Both mIPSC frequency and amplitude were significantly reduced in NPAS4-KO CA1 pyramidal neurons from animals injected with KA compared to mice maintained in standard housing (**Figure 6**, freq: $p<0.01$, amp: $p<0.05$). These data indicate that the difference in mIPSC frequency and amplitude measured in NPAS4-KO relative to NPAS-WT neurons is primarily due to the disruption of NPAS4 function in excitatory neurons.

**Npas4 differentially regulates inhibitory synapses across the somato-dendritic axis**

Since mIPSCs reflect synaptic transmission that can occur throughout the neuron, albeit with a bias towards more proximal synapses (Cossart et al., 2000), the NPAS4-dependent decreases in mIPSC frequency and amplitude we observe could result from homeostatic regulation of all inhibitory synapses or from modification of inhibitory synapses that form on discrete

regions of the pyramidal neuron – possibilities that are not distinguishable by measuring mIPSCs alone. Although inhibitory neurons are quite heterogeneous, individual inhibitory neuron subtypes have axons that elaborate preferentially in one or more hippocampal layers in a stereotyped manner(Danglot et al., 2006; T.F. Freund, 1996). Thus, stimulation of axons in the different laminar domains of the hippocampus and analysis of the resulting inhibitory currents has the potential to reveal whether the NPAS4-dependent effects on inhibition are due to homeostatic scaling of inhibitory synapses or to changes in inhibitory synapses on discrete regions of pyramidal neurons.

To determine if NPAS4 regulates all or subsets of inhibitory synapses made onto the postsynaptic pyramidal neuron, we sparsely excised Npas4 as described above and made direct comparisons of layer-specific, pharmacologically isolated, monosynaptic evoked inhibitory postsynaptic currents (eIPSCs) recorded simultaneously from neighboring NPAS-KO and NPAS4-WT CA1 neurons (**Figure 7**). Extracellular stimulation of local axons within specific lamina of the hippocampus was delivered by current injection through a theta glass stimulating electrode that was placed in the center of the relevant layer along the somato-dendritic axis of the CA1 neuron. The stimulus strength was the minimum required to generate an eIPSC in both NPAS4-KO and NPAS4-WT neurons. Recording from neighboring neurons increased the probability that these neurons receive synaptic input from the same population of inhibitory axons while simultaneous recordings insured that the neighboring NPAS4-KO and NPAS4-WT neurons were exposed to an identical extracellular stimulus. For each eIPSC recorded, the slope of the

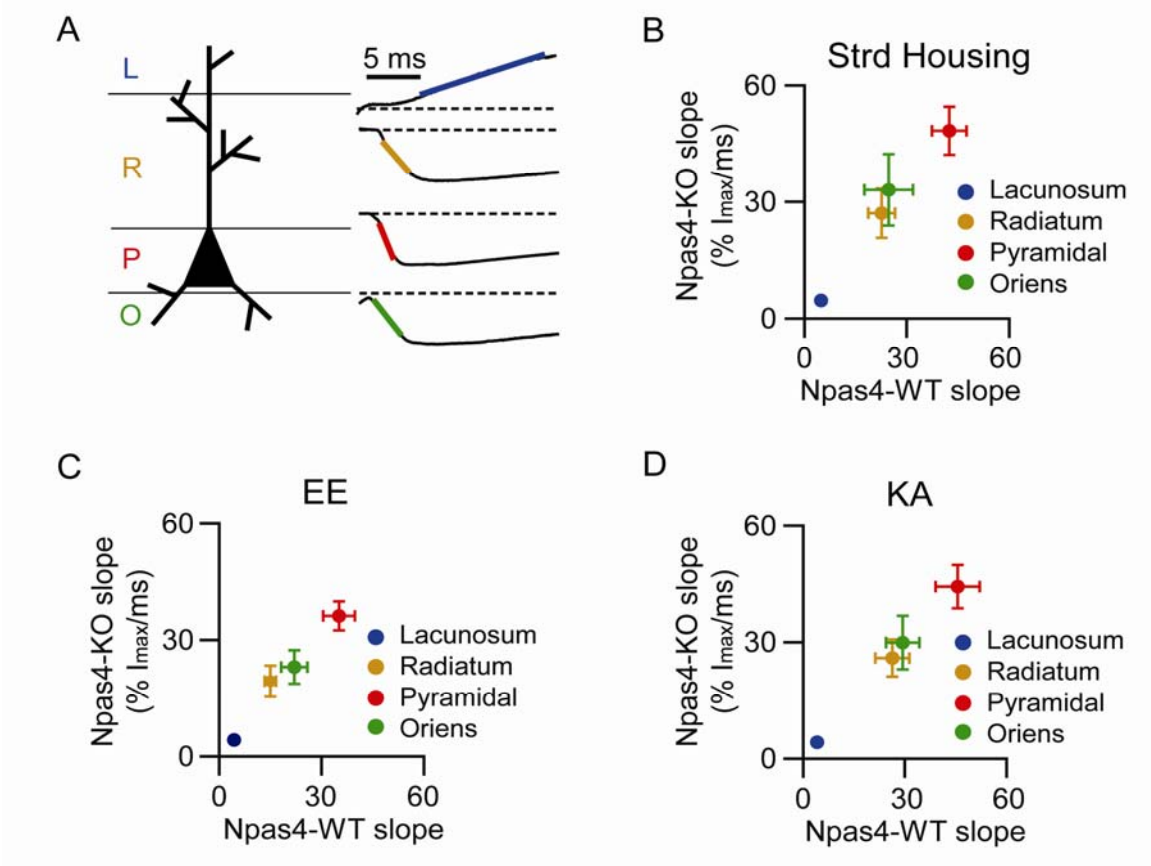


**Figure 8. Stimulation of axons in different hippocampal layers generates eIPSCs with distinct rise times.**

(A) Cartoon of a CA1 pyramidal neuron and example eIPSCs generated in response to stimulation of axons in lacunosum-moleculare (L, blue), radiatum (R, yellow), pyramidale (P, red), and oriens (O, green). Slopes (10-90% of the peak eIPSC) are indicated by colored lines.

(B) Standard housing conditions – Summary of the slopes of the eIPSC rise times recorded from neighboring NPAS4-WT and NPAS4-KO neurons in response to stimulation of axons in each of the four hippocampal layers. These data are from the eIPSCs shown in Figure 2B-E.

**Figure 8 (Continued)**. (C) Enriched Environment – Summary of the slopes of the eIPSC rise times recorded from neighboring NPAS4-WT and NPAS4-KO neurons in response to stimulation of axons in in each of the four hippocampal layers. These data are from the eIPSCs shown in Figure 2F-I.

(D) Kainic Acid – Summary of the slopes of the eIPSC rise times recorded from neighboring NPAS4-WT and NPAS4-KO neurons in response to stimulation of axons in in each of the four hippocampal layers. These data are from the eIPSCs shown in Supplemental Figure 5B-E. Significance was determined by two-tailed t-test.

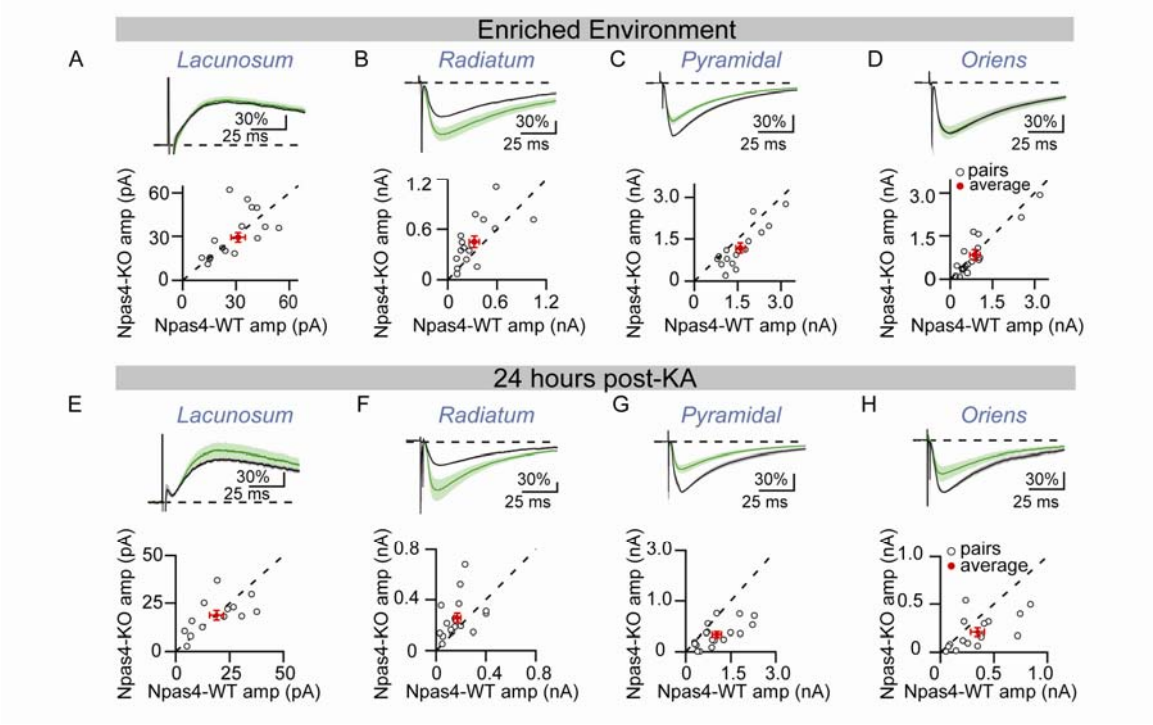


**Figure 9. NPAS4 differentially regulates inhibitory synapse function across the somato-dendritic axis of pyramidal neurons in response to exploration of an enriched environment.**

Experimental configuration is identical to Figure 4. A stimulating electrode was placed in one of the four layers of CA1 and local axons depolarized. eIPSCs were measured simultaneously from neighboring NPAS4-WT (black) and NPAS4-KO (green) neurons. Layers - L: lacunosum-moleculare, R: radiatum, P: pyramidale, O: oriens.

(A-D) eIPSCs measured from mice exposed to enriched enviornment. Top: Normalized, average eIPSC measured from NPAS4-WT (black) and NPAS4-KO (green) neurons in response to stimulation of axons in (B) lacunosum-molecular, (C) radiatum, (D) pyramidale, or (E) oriens are shown. Currents were normalized pairwise to the peak of

**Figure 9 (Continued)**. the NPAS4-WT eIPSC. Data are shown as the mean (line) ± SEM (shaded region). Scale bars: 30% change in normalized current, 25 ms. Bottom: eIPSC amplitude measured from pairs of neighboring NPAS4-KO and NPAS4-WT neurons in response to stimulation of axons in (B) lacunosum-molecular, (C) radiatum, (D) pyramidale, or (E) oriens. Open circles indicate individual NPAS4-KO/NPAS4-WT pairs. Red circles indicate the mean ± SEM.

(F-I) eIPSCs measured from mice exposed to kainic acid. Top: Normalized, average eIPSC measured from NPAS4-WT (black) and NPAS4-KO (green) neurons in response to stimulation of axons in (F) lacunosum, (G) radiatum, (H) pyramidale, or (I) oriens are shown. Currents were normalized pairwise to the NPAS4-WT peak eIPSC. Data are shown as the mean (line) ± SEM (shaded region). Scale bars: 30% change in normalized current, 25 ms. Bottom: eIPSC amplitude measured from pairs of neighboring NPAS4-KO and NPAS4-WT neurons in response to stimulation of axons in (F) lacunosum, (G) radiatum, (H) pyramidale, or (I) oriens. Open circles indicate individual NPAS4-KO/NPAS4-WT pairs. Red circles indicate the mean ± SEM.

rise time was measured (10-90% of the peak). As predicted by cable properties, the eIPSC slope correlated with distance of the stimulating electrode from the recording electrode such that stimulation of axons in stratum pyramidale generated eIPSCs with faster rise times than those recorded from stimulation in oriens and radiatum, which in turn were faster than those recorded from stimulation in lacunosum-moleculare (**Figure 8**). This indicates that stimulation of axons within a given layer is predominately activating synapses within that layer (Miles and Poncer, 1996; Miles et al., 1996).

We found that in slices obtained from mice housed in a standard environment, where NPAS4 is not induced and NPAS4-dependent changes in mIPSCs are not detected, equivalent eIPSCs were recorded from NPAS4-WT and NPAS4-KO neurons in response to stimulation of axons in any hippocampal layer (**Figure 7**). However, in slices obtained from mice exposed to an enriched environment, extracellular stimulation of axons in the pyramidal layer generated smaller eIPSCs in NPAS4-KO neurons than in the neighboring NPAS4-WT neurons (**Figure 9**, $p<0.001$). These findings are consistent with the EE-dependent decreases in mIPSC frequency and amplitude observed in NPAS4-KO neurons compared to NPAS4-WT neurons. We next stimulated axons within each of the layers of neuropil. In contrast to our findings in the pyramidal layer, upon stimulation of axons in stratum radiatum significantly larger eIPSCs were recorded from NPAS4-KO neurons than neighboring NPAS4-WT neurons (**Figure 9**, Supplemental Table 2, $p<0.05$) while no difference was detected between NPAS4-WT and KO neurons in response to stimulation of axons in

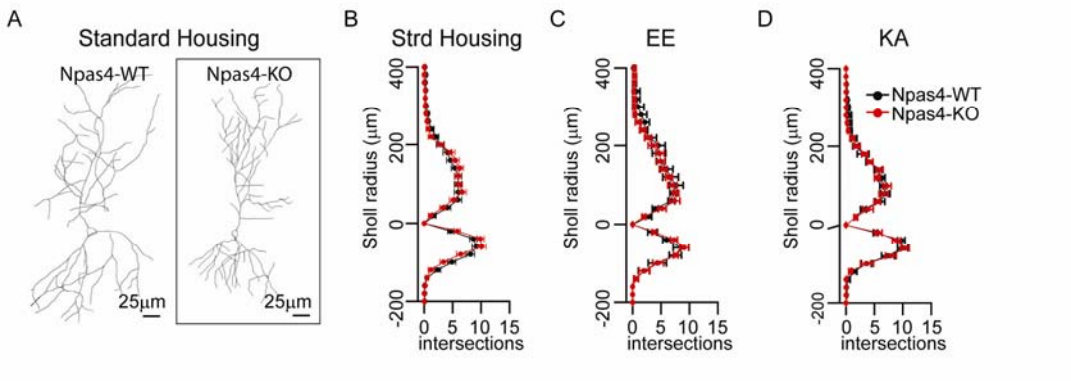


**Figure 10. Sholl analysis shows no alteration in dendritic complexity resulting from Npas4 deletion.**

(A) Example of skeletonized NPAS4-WT and NPAS4-KO CA1 pyramidal neurons from mice injected with KA (left). CA1 region of hippocampus was infected with an AAV encoding a YFP which was used for dendritic visualization. (B) Quantification of the number of dendrites at increasing Sholl radii from NPAS4-WT(black) or NPAS4-KO (red) neurons (right). Data are shown as the mean ± SEM. Significance was determined by ANOVA, p=0.92.

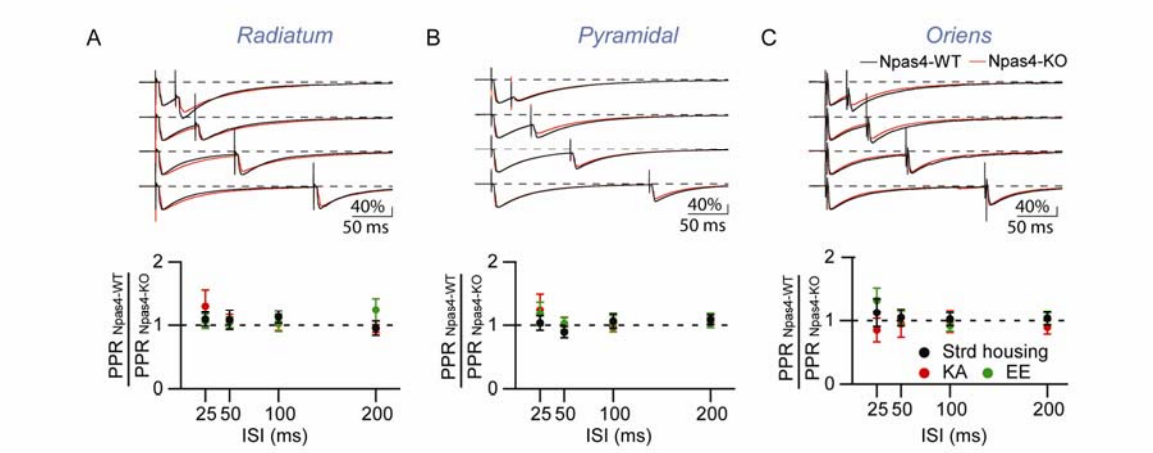


**Figure 11. Pair pulse ratios are unaltered in Npas4 KO neurons**

(A-C) Comparison of paired pulse ratios measured from neighboring NPAS4-WT and NPAS4-KO neurons in response to stimulation of axons in (A) radiatum, (B) pyramidale, or (C) oriens from mice housed in standard conditions (black) or injected with KA (green). Data are shown as the PPRNPAS4-WT/PPRNPAS4-KO mean ± SEM. Significance was determined by ANOVA, Dunnett's test compared with standard housing $p > 0.05$ for all layers, conditions, and ISIs.

oriens or lacunosum (**Figure 9**). Similar results were obtained if instead of exposure to an enriched environment, the mice were injected with KA to induce NPAS4 (**Figure 9**). Taken together these findings suggest that NPAS4 expression does not result in uniform, homeostatic regulation of inhibitory synapses. Rather, NPAS4 functions in an unprecedented manner, simultaneously decreasing inhibition within the proximal apical dendrites while increasing inhibition at the soma.

Extracellular stimulation of axons could result in the depolarization of axons of passage that form synapses in regions other than the intended layer. To address this possibility we compared the rise times of the eIPSCs recorded from NPAS4-WT and NPAS4-KO neurons and found them to be indistinguishable (**Figure 8**). This indicates that the redistribution of inhibition observed is not due to a bias in synaptic transmission associated with axons of passage onto NPAS4-WT or KO neurons. Additionally, the hippocampus contains many interneurons that synapse in multiple layers (i.e. bistratified and trilaminar cells). If axons from these cell types form NPAS4-regulated synapses onto CA1 pyramidal neurons, then the absence of an NPAS4 phenotype upon stimulation within oriens suggests the effect of NPAS4 disruption is localized to individual synapses and does not occur at all synapses made by a given axon.

**Characterization of Npas4-dependent regulation of inhibition across the somato-dendritic axis**

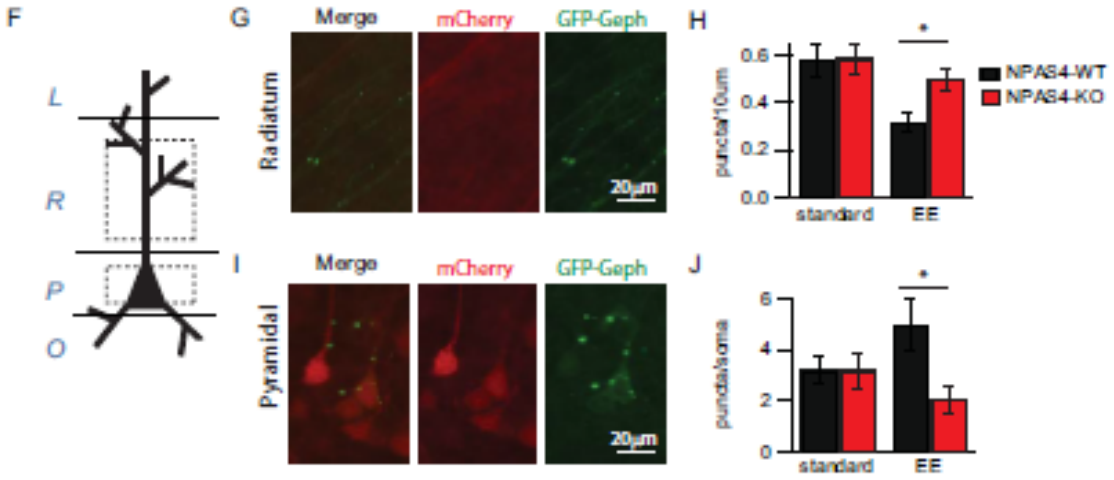


**Figure 12. Npas4 regulates inhibitory synapse number in vivo in response to experience.**

(F) Schematic of the regions imaged for GFP-gephyrin quantification.

(G) Example image from stratum radiatum. mCherry is in red and GFP-gephyrin is in green. Scale bar = 20μm.

(H) Quantification of puncta per 10 μm observed on dendrites in stratum radiatium from NPAS4-WT (black) and NPAS4-KO (red) neurons. Data are shown as the mean ± SEM. Significance was determined by ANOVA, * $p<0.05$

(I) Example image from stratum pyramidale. mCherry is in red and GFP-gephyrin is in green. Scale bar = 20μm.

(J) Quantification of puncta per soma in stratum pyramidale from NPAS4-WT (black) and NPAS4-KO (red) neurons. Data are shown as the mean ± SEM. Significance was determined by ANOVA, * $p<0.05$

We next investigated the cellular mechanisms by which NPAS4 differentially regulates inhibition on hippocampal pyramidal neurons, including possible effects on dendritic growth, changes in the probability of inhibitory synaptic vesicle release, or changes in inhibitory synapse number. We first asked if loss of NPAS4 results in altered dendritic complexity which could indirectly lead to larger eIPSCs in response to stimulation of axons in stratum radiatum either by providing more surface area for synapses to form or by reducing the capacitance of the cell. This seems unlikely since Sholl analysis revealed that the disruption of NPAS4 function has no effect on the number or length of apical or basal dendrites (**Figure 10**) or on the cell capacitance of neurons in mice housed under standard conditions, in an enriched environment, or exposed to KA .

We next asked if disruption of Npas4 leads to changes in presynaptic release of neurotransmitter at axons that synapse onto different regions of the pyramidal neuron. We measured the paired pulse ratios (PPRs) upon stimulation of axons in each of the hippocampal layers, and compared NPAS-WT and NPAS-KO neurons in slices obtained from mice housed under standard conditions or exposed to EE or KA. We found no difference between the PPRs of NPAS-WT and NPAS4-KO neurons under any of these conditions (**Figure 11**) indicating that the NPAS4-dependent changes in eIPSCs are not likely due to changes in the probability of presynaptic release.

| gene | chr | pos | induction of gene | induction at peak |
|---|---|---|---|---|
| 4921504E06Rik | 2 | 19476120 | 8 | 6.2 |
| 9530008L14Rik | 13 | 41896890 | 8.6 | 21 |
| Abcd2 | 15 | 90983260 | 2.48429 | 5.5 |
| Adcyap1 | 17 | 93602815 | 4.33656 | 5.929 |
| Ankrd56 | 5 | 93483350 | 15.9545 | 11 |
| Arhgap29 | 3 | 121676880 | 3.56853 | 5.429 |
| Bdnf | 2 | 109532475 | 35.2919 | 205.333 |
| Bdnf | 2 | 109518455 | 35.2919 | 4.333 |
| Bdnf | 2 | 109514675 | 35.2919 | 128 |
| Cd6 | 19 | 10859575 | 2.11111 | 7.5 |
| Cpa4 | 6 | 30522930 | 5.70588 | 25.5 |
| Cpxm2 | 7 | 139350455 | 2.56693 | 6.286 |
| Crem | 18 | 3281155 | 5.14777 | 16.8 |
| Crem | 18 | 3281830 | 5.14777 | 22 |
| Cyr61 | 3 | 145314740 | 4.5102 | 6 |
| D16Ertd472e | 16 | 78576220 | 5.54462 | 12 |
| D3Bwg0562e | 3 | 117060470 | 4.03298 | 10 |
| Dbc1 | 4 | 68615695 | 4.20687 | 5.005 |
| Ddx3y | 21 | 622975.5 | 3.93276 | 10 |
| Dkk2 | 3 | 131749835 | 9.25532 | 10.5 |
| Dusp6 | 10 | 98786170 | 2.54083 | 9 |
| E430004N04Rik | 10 | 28532080 | 8.13043 | 13 |
| Fer1l3 | 19 | 38066355 | 5.39535 | 74 |
| Fer1l3 | 19 | 37982665 | 5.39535 | 9 |
| Fos | 12 | 86812870 | 33.5814 | 14 |
| Fosb | 7 | 19905495 | 53 | 5.333 |
| Fosb | 7 | 19894115 | 53 | 20 |
| Fosl2 | 5 | 32435940 | 5.29613 | 14 |
| Fosl2 | 5 | 32438065 | 5.29613 | 5.875 |
| Gabra4 | 5 | 72008145 | 3.34333 | 5.5 |
| Gabrb1 | 5 | 72460260 | 2.17759 | 6 |
| Gcnt2 | 13 | 41013390 | 3.71429 | 6.2 |
| Gpr22 | 12 | 32394835 | 5.68515 | 7.676 |
| Gpr3 | 4 | 132767740 | 10.1849 | 15 |
| Hcn1 | 13 | 118394055 | 2.98126 | 5.5 |
| Hdac9 | 12 | 35213780 | 8.31166 | 9.947 |
| Hdac9 | 12 | 35214265 | 8.31166 | 9.915 |
| Hdac9 | 12 | 35182840 | 8.31166 | 5 |
| Hdac9 | 12 | 35166755 | 8.31166 | 24.75 |
| Hdac9 | 12 | 35183850 | 8.31166 | 18 |
| Hdac9 | 12 | 35173085 | 8.31166 | 5.31 |
| Hspb3 | 13 | 114453860 | 11.2703 | 10.947 |
| Hunk | 16 | 90387145 | 2.93033 | 5 |
| Iqsec3 | 6 | 121423910 | 2.03163 | 7.009 |
| Junb | 8 | 87502555 | 18.6986 | 19.684 |
| Kcna4 | 2 | 107257495 | 3.2902 | 8.857 |
| Kcnj3 | 2 | 55289600 | 5.1252 | 6.675 |
| Klhl4 | 20 | 111587385 | 6.72727 | 5.889 |
| Maff | 15 | 79177910 | 10.8679 | 14 |
| Maff | 15 | 79178470 | 10.8679 | 6.5 |

| gene | chr | pos | induction of gene | induction at peak |
|---|---|---|---|---|
| Maml3 | 3 | 51906195 | 3.28369 | 5.75 |
| Maml3 | 3 | 51907390 | 3.28369 | 11.333 |
| Mest | 6 | 30695130 | 4.66716 | 6.274 |
| Myo3b | 2 | 69952395 | 2.02105 | 5 |
| Nfil3 | 13 | 53078245 | 4.87197 | 12.32 |
| Npas4 | 19 | 4989805 | 73.8489 | 58.538 |
| Npas4 | 19 | 4993095 | 73.8489 | 19 |
| Nptx2 | 5 | 145308275 | 7.35033 | 9.568 |
| Nr4a1 | 15 | 101097330 | 36.0876 | 66.4 |
| Nr4a2 | 2 | 56969220 | 6.71864 | 10.25 |
| Nr4a3 | 4 | 48057945 | 12.8444 | 10.559 |
| Nr4a3 | 4 | 48056410 | 12.8444 | 11.375 |
| Nr4a3 | 4 | 48057290 | 12.8444 | 12.034 |
| Olfml2a | 2 | 38806110 | 2.34211 | 17 |
| Pacsin3 | 2 | 91095860 | 2.12644 | 15 |
| Pam | 1 | 99928620 | 3.52883 | 11.647 |
| Pappa | 4 | 64788065 | 2.88618 | 8 |
| Pcdh11x | 20 | 117723835 | 2.41197 | 9 |
| Pcsk1 | 13 | 75228705 | 37.6 | 13.1 |
| Pde4d | 13 | 110612880 | 2.31523 | 50 |
| Penk1 | 4 | 4065825 | 2.1 | 5.231 |
| Per1 | 11 | 68913080 | 3.159 | 7.8 |
| Rabggtb | 3 | 153574995 | 3.08718 | 6.065 |
| Rgs2 | 1 | 145852135 | 8.16283 | 10.181 |
| Rgs2 | 1 | 145851380 | 8.16283 | 7.207 |
| Rgs2 | 1 | 145850695 | 8.16283 | 8.76 |
| Rspo3 | 10 | 29259485 | 2.27746 | 6 |
| Scn1a | 2 | 66246895 | 2.98474 | 6.875 |
| Sertad1 | 7 | 28271930 | 9.30631 | 7.526 |
| Slc6a17 | 3 | 107319165 | 2.54003 | 5 |
| Snx7 | 3 | 117526220 | 2.07258 | 5.5 |
| Snx7 | 3 | 117529915 | 2.07258 | 6.5 |
| Sorcs3 | 19 | 48315650 | 2.76436 | 11 |
| Sorcs3 | 19 | 48659720 | 2.76436 | 5.5 |
| Sorcs3 | 19 | 48172075 | 2.76436 | 8 |
| Spry2 | 14 | 106297475 | 2.01437 | 14.75 |
| Stac | 9 | 111591890 | 3.65815 | 5.083 |
| sult2b1 | 13 | 96731800 | 4.05891 | 9 |
| Sv2c | 3 | 93251570 | 2 | 7 |
| Tchh | 8 | 66685070 | 6.68364 | 5.579 |
| Tll1 | 9 | 53914130 | 2.51701 | 5.75 |
| Tnfaip8l3 | 1 | 162079810 | 11.2174 | 13 |
| Tnn | 9 | 8544010 | 8.38462 | 17 |
| Trpc6 | 6 | 30871095 | 5.66667 | 6.75 |
| Tsga13 | 6 | 30871525 | 5.66667 | 6 |
| Tsga13 | 6 | 30858185 | 5.66667 | 12 |
| Tsga13 | 8 | 74194390 | 2.24115 | 5.667 |
| Unc13a | 5 | 137505265 | 13.7907 | 10.625 |
| Vgf | 5 | 137506375 | 13.7907 | 14.077 |
| Vgf | 9 | 119920665 | 13.7907 | 6.8 |

**Figure 13. Putative Npas4 targets identified by genome-wide analysis**

Finally we sought to determine if NPAS4 could be differentially regulating the number of inhibitory synapses formed onto the cell body or apical dendrites. To quantify inhibitory synapses within these domains, we stereotaxically injected two AAVs, one encoding the red fluorescent protein mCherry followed by an IRES sequence and Cre (AAV-mCherry-IRES-Cre) and the second encoding a double floxed inverted GFP-gephyrin fusion protein (dfi-GFP-gephyrin), into the CA1 region of the hippocampus in wild type and $Npas4^{f/f}$ mice (P13-15). GFP-gephyrin fusion proteins have been previously shown to localize to inhibitory synapses and without significantly altering neurotransmission (Chen et al., 2012; Versendaal et al., 2012). Using this strategy allowed us to sparsely manipulate NPAS4 expression and quantify GFP-gephyrin puncta specifically on NPAS4-WT and NPAS4-KO neurons. This analysis revealed that when mice were kept in standard housing NPAS4-WT and NPAS4-KO hippocampal pyramidal neurons have equivalent densities of GFP-gephyrin puncta on the soma and apical dendrites. However, after exposure to an enriched environment, NPAS4-KO pyramidal neurons have significantly fewer somatic and more dendritic GFP-gephyrin puncta than NPAS4-WT neurons (**Figure 12**, EE soma: $p<0.01$, dendrites: $p<0.05$). These findings, together with the electrophysiology data described above, indicate that when exposed to an enriched environment, NPAS4-KO CA1 pyramidal neurons have fewer functional inhibitory synapses on their soma and a greater number of functional inhibitory synapses on their apical dendrites in comparison to wild type neurons. Strikingly, comparison of the

number of GFP-gephyrin puncta measured on wild type neurons from mice housed in standard versus enriched environments revealed that

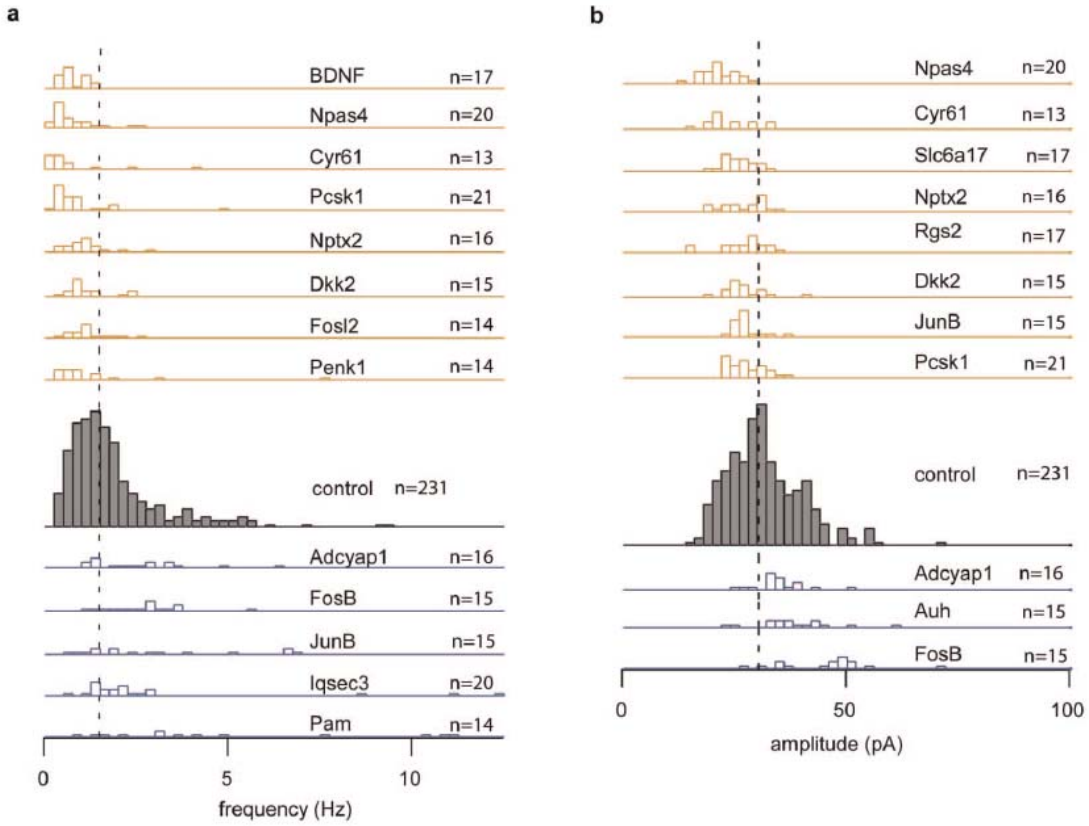


**Figure 14. Functional screen of putative Npas4 target genes identifies many genes that regulate mIPSC frequency and amplitude.**

(A,B) mIPSCs were recorded from CA1 pyramidal neurons transfected with a pool of three shRNAs targeting a single putative NPAS4 target gene. mIPSC frequency (A) amplitude (B) of those significantly different from control are shown. Knockdown of genes that result in fewer or smaller mIPSCs are shown on top (mustard); knockdown of genes that result in more or larger mIPSCs are shown on the bottom (blue). The dashed line represents the median value from control conditions. $P < 0.05$.

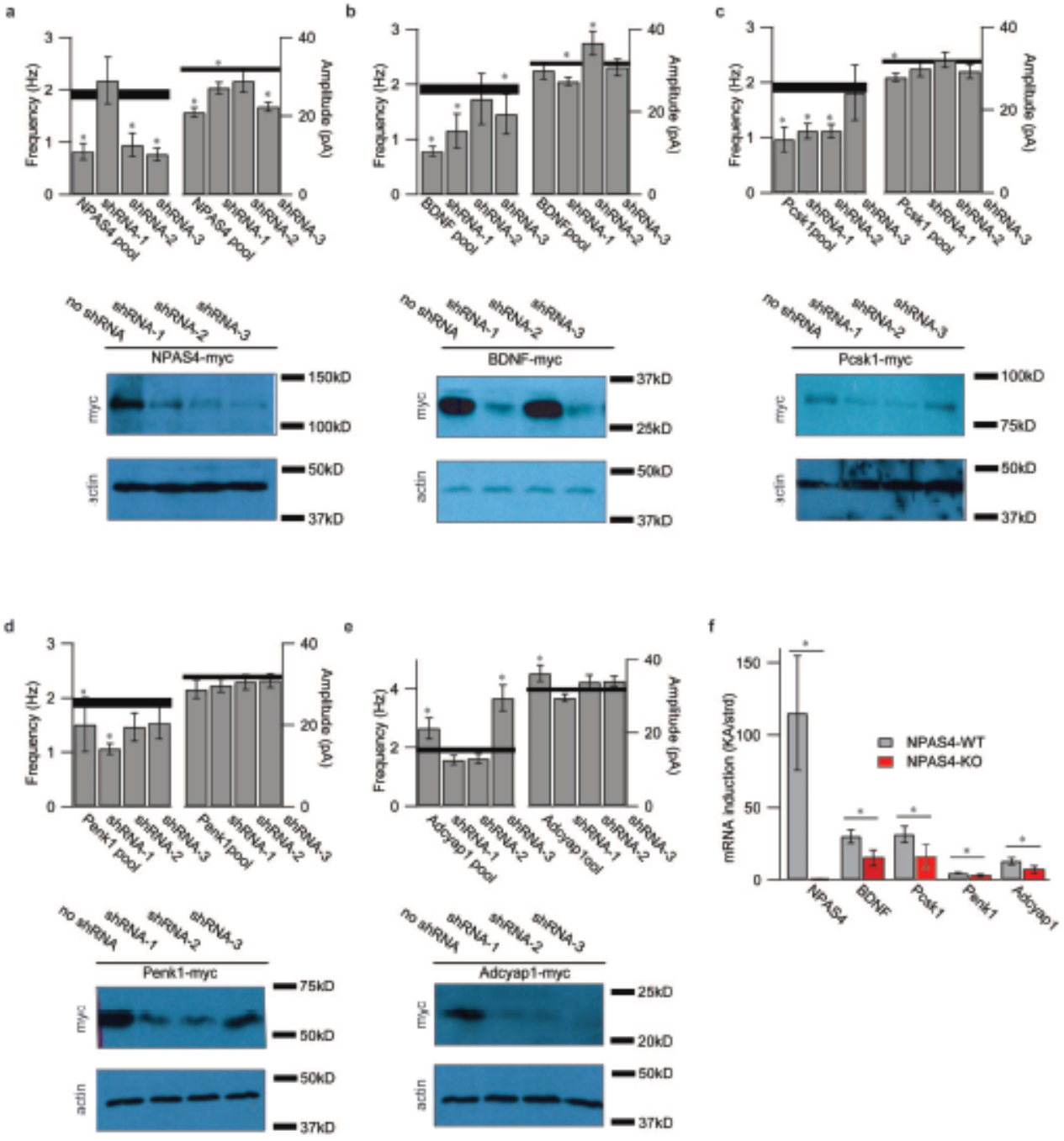


**Figure 15. Validation of five putative NPAS4 target genes.**

**Figure 15 (Continued)**. Select putative NPAS4 target genes that influence mIPSC frequency and/or amplitude were subjected to additional validation: (A) NPAS4, (B) BDNF, (C) Pcsk1, (D) Penk1, and (E) Adycap1. First, organotypic hippocampal slice cultures were transfected with individual shRNAs from the original pool of three used in the primary screen. Whole-cell voltage clamp recordings were made from transfected CA1 pyramidal neurons and mIPSCs recorded. This analysis revealed that from each pool, expression of one or two shRNAs phenocopied the pool of shRNAs. Second, HEK 293T cells were transfected with myc-tagged versions of the putative target gene and a shRNA targeting that gene. One day later, the cells were lysed and the lysates probed for myc by Western blot analysis. This analysis revealed that multiple shRNAs were capable of reducing expression of the intending protein. Finally, qPCR was performed on cDNA generated from hippocampi from NPAS4 wild type and knockout mice that were maintained in a standard environment or injected with KA. This analysis demonstrated that all 5 putative target genes are induced in vivo and that this induction is misregulated in NPAS4 knockout neurons.

exposure to an EE leads to an increase in the number of somatic and a decrease in the number of dendritic inhibitory synapses. In both domains of the neuron behaviorally-triggered changes in inhibition are NPAS4 dependent. These findings suggest that sensory input, by activating NPAS4 transcription, promotes plasticity within neural circuits by specifically enhancing somatic inhibition while relieving dendritic inhibition.

**Screening for Npas4 targets reveals novel molecules in the activity-dependent**

NPAS4 is a transcription factor, and thus to understand how it mediates sensory-dependent changes in inhibitory synapse number we sought to identify NPAS4 target genes and assess their function. We focused our attention on putative NPAS4 targets that satisfy three criteria: 1) NPAS4 is bound within 10 kB of the gene, 2) mRNA transcribed near the NPAS4 peak is induced greater than five-fold and the gene is induced at least 2 fold in response to membrane depolarization, and 3) in organotypic slice culture, shRNA knock-down of the mRNA transcribed from the gene locus, results in a statistically significant change in mIPSCs. To identify genes that fulfill these three criteria we analyzed available NPAS4 ChIP-seq and RNA-seq data (Kim et al., 2010) obtained from unstimulated and membrane depolarized neurons (**Figure 13**), and then evaluated a subset of the genes that fulfilled the first two criteria, one by one, using the electrophysiology-based assay of functional inhibitory synapses. Through this screen we identified 16 putative NPAS4 targets that display an increase or decrease in mIPSC frequency or amplitude when their expression is knocked-down with gene specific

shRNAs in organotypic hippocampal slices (**Figure 14**), five of which we further validated (**Figure 15**).

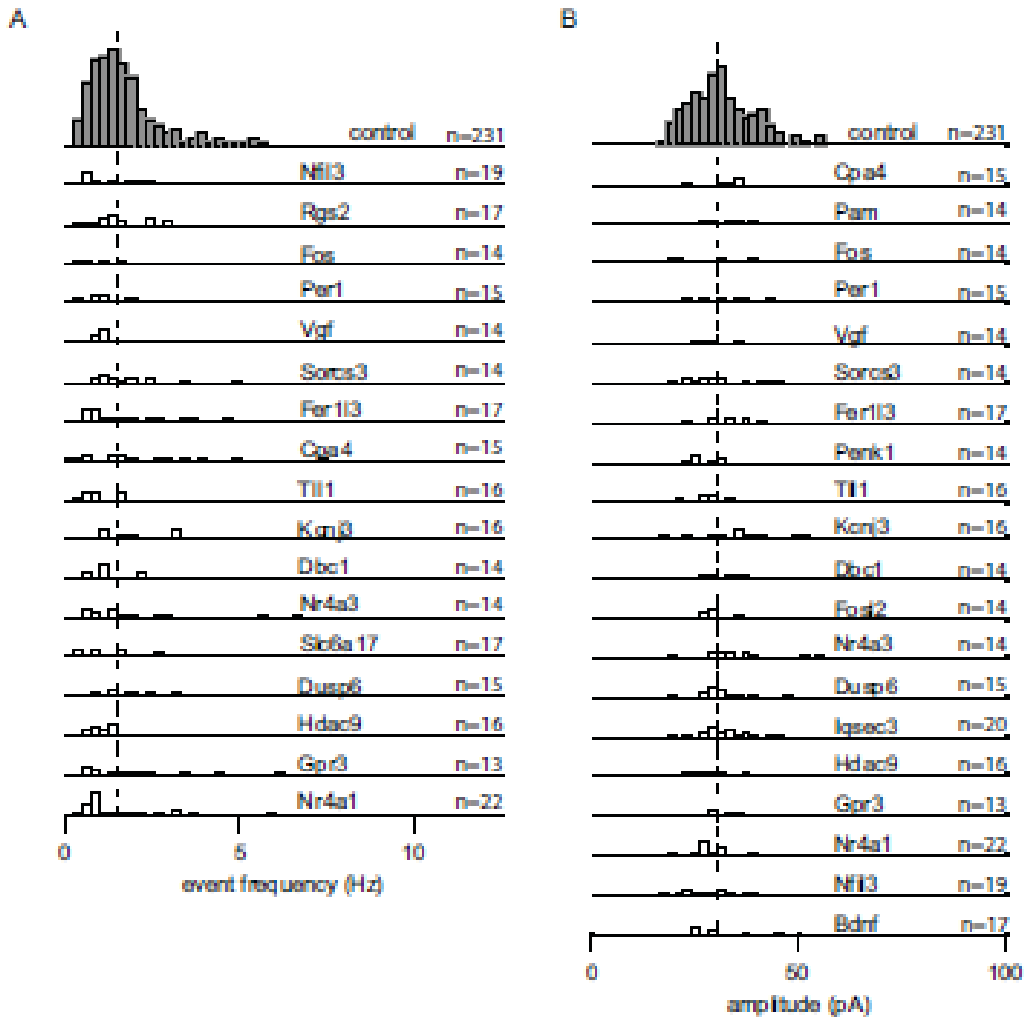


**Figure 16. Not all putative NPAS4 target genes regulate mIPSCs frequency or amplitude.**

(A-B) mIPSCs were recorded from CA1 pyramidal neurons transfected with a pool of three shRNAs targeting a single putative NPAS4 target gene. mIPSC frequency (A) and

**Figure 16 (Continued)**. amplitude (B) of those not significantly difference from control are shown. Significance was determined by Wilcoxon rank sum test. $p>0.05$.

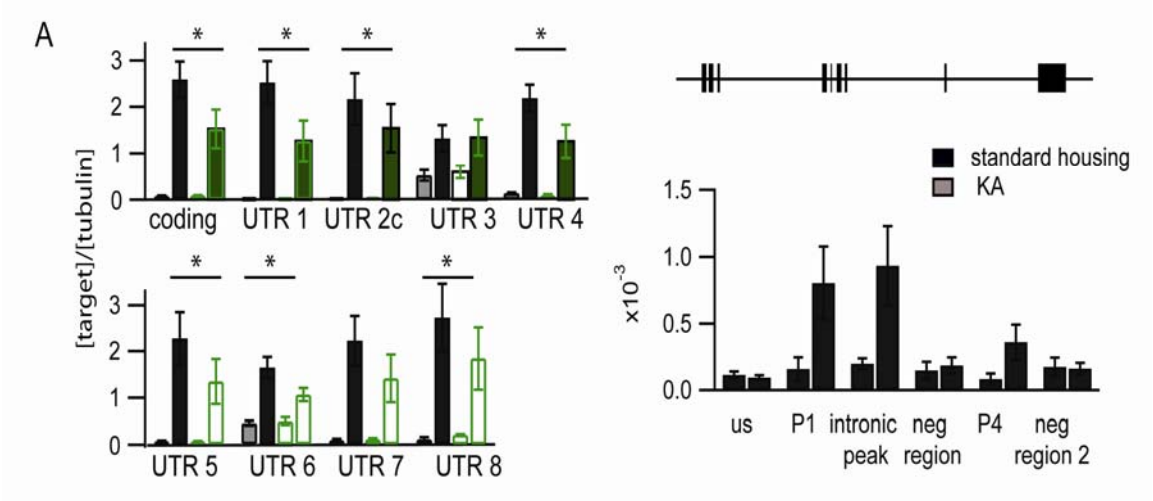


**Figure 17. Npas4 regulates BDNF mRNA and is bound to the promoter and enhancer of BDNF after neuronal activity.**

(A) Schematic of the BDNF genomic locus. Each exon, 1-9, is indicated. Nuclei were collected from wild type mice in standard conditions (black) or after injection with KA (red). NPAS4-bound DNA was immunoprecipitated and quantified with qPCR. us: upstream region, P1: promoter 1, I3: intron 3, neg 1: control negative region within intron 1, P4: promoter 4, neg 2: control negative region within intron 7. Enrichment is shown relative to the input DNA. * $p<0.05$ two tailed t-test. Induction of each of the BDNF exons in the hippocampus of wild type (black) or NPAS4 knockout (green) mice as measured by qPCR using primers specific to each exon, E1-9. Significance was determined by two-tailed t-test. * $p<0.05$, # $p=0.05$.

Notably, not all molecules identified by the screening strategy showed an alteration in mIPSC frequency or amplitude (**Figure 16**).

**The Npas4 target BDNF specifically regulates somatic inhibition in an activity-dependent manner *in vivo***

Of the putative NPAS4 targets identified by the screen, BDNF, seemed one of the most likely candidates to control the number of inhibitory synapses that form on a specific region of an excitatory neuron in response to sensory stimulation. BDNF expression is regulated by neuronal activity in vivo (Castren et al., 1996; Edward S. Lein, 2000; Falkenberg et al., 1992; Rocamora et al., 1996) and controls the number and strength of inhibitory synapses that form on pyramidal neurons (Baldelli et al., 2005; Kohara et al., 2007; Marty et al., 2000). In addition, particular BDNF mRNAs have been shown to be targeted to discrete regions of the neuron (Pattabiraman et al., 2005), and BDNF containing vesicles are known to be secreted from the axon, soma, or dendrites of pyramidal neurons (Brigadski et al., 2005; Dean et al., 2012). Furthermore, we confirmed by chromatin immunoprecipitation and qPCR that NPAS4 binds to three sites within the BDNF gene (**Figure 17**), and that KA induction of transcription of multiple BDNF isoforms is significantly reduced in the hippocampus of NPAS KO compared to wild type mice (**Figure 17**).

To determine if BDNF is a target of NPAS4 that selectively regulates somatic and/or dendritic inhibition of pyramidal neurons in vivo we injected AAV-Cre-GFP into BDNF

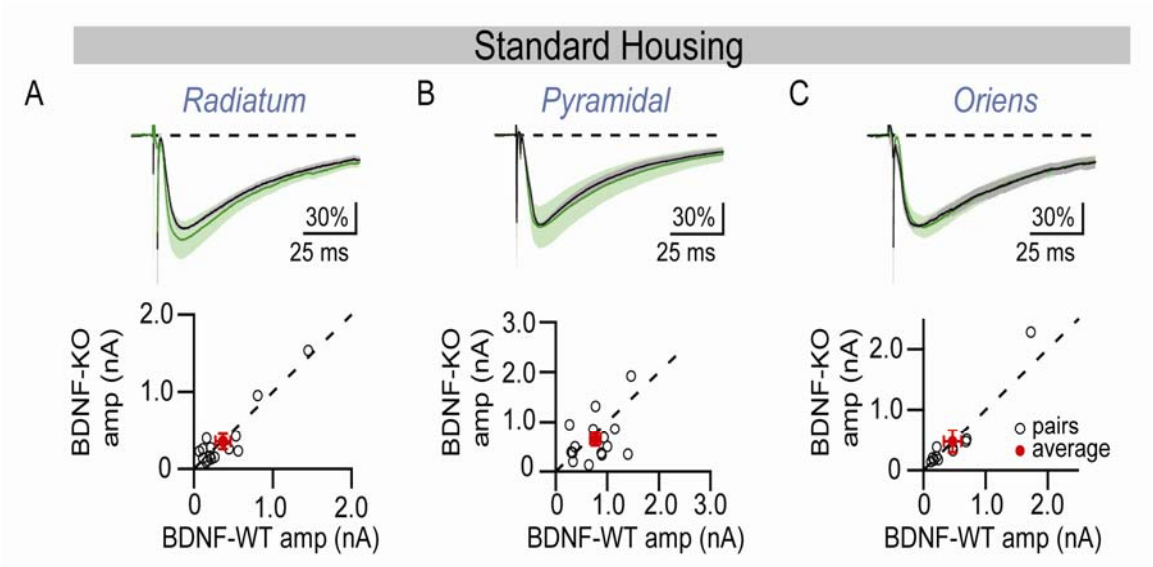


**Figure 18. BDNF does not regulate inhibition across the somatodendritc axis in mice maintained in standard housing conditions.**

(A-C) eIPSCs measured from mice maintained in standard housing. Top: Normalized, average eIPSC measured from BDNF-WT (black) and BDNF-KO (green) neurons in response to stimulation of axons in (A) radiatum, (B) pyramidale, or (C) oriens are shown. Data are shown as the mean (line) ± SEM (shaded region). Scale bars: 30% change in normalized current, 25 ms. Bottom: eIPSC amplitude measured from pairs of neighboring BDNF-KO and BDNF-WT neurons in response to stimulation of axons in (A) radiatum, (B) pyramidale, or (C) oriens. Open circles indicate individual BDNF-KO/BDNF-WT pairs. Red circles indicate the mean ± SEM. Significance was determined by paired two-tailed t-test.

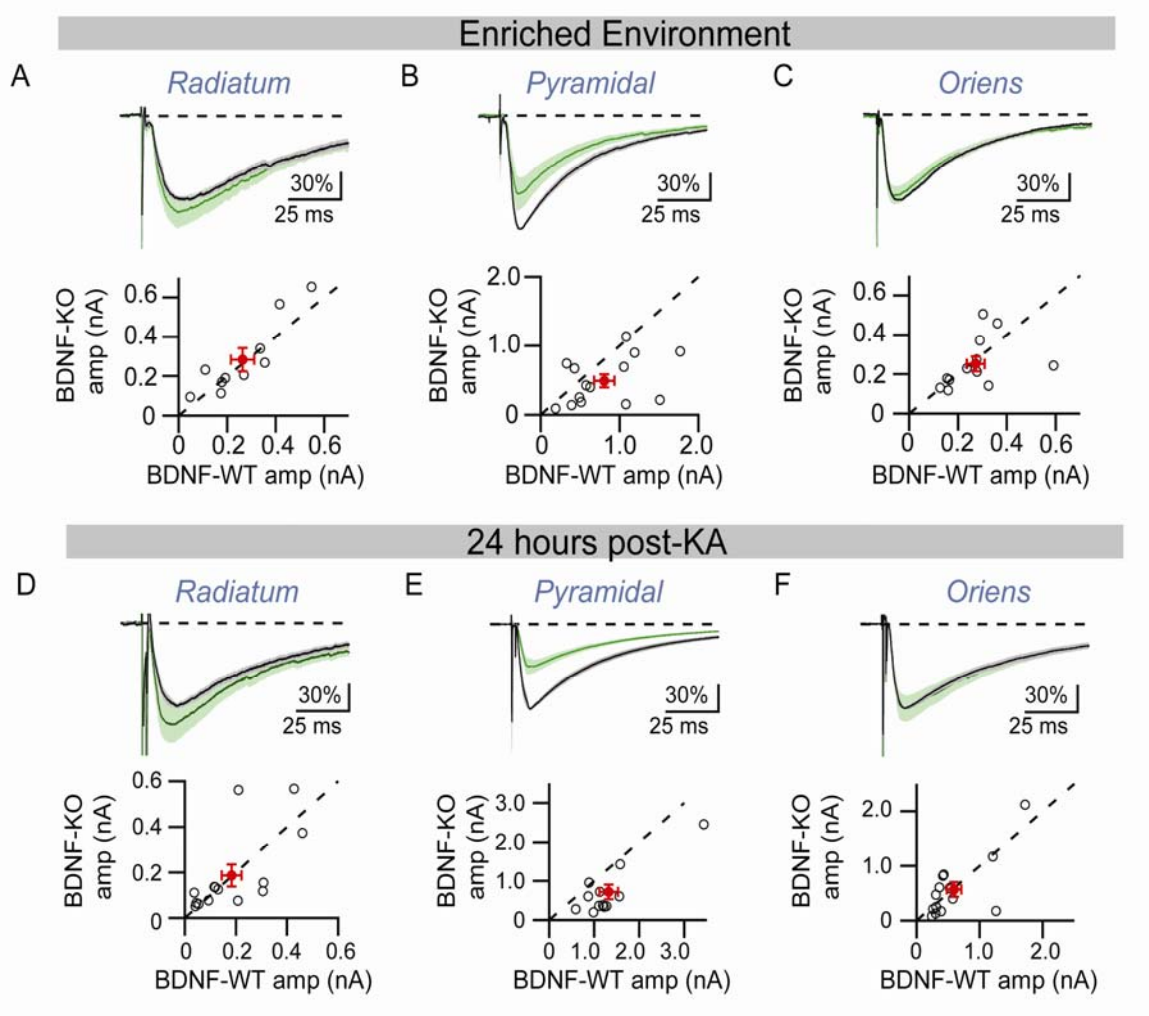


**Figure 19. BDNF regulates somatic, but not dendritic, inhibition on CA1 pyramidal neurons in an activity-dependent manner.**

(A-C) eIPSCs measured from mice exposed to enriched environment from 4-10 days. Top: Normalized, average eIPSC measured from BDNF-WT (black) and BDNF-KO (green) neurons in response to stimulation of axons in (A) radiatum, (B) pyramidale, or (C) oriens are shown. Data are shown as the mean (line) ± SEM (shaded region). Scale bars: 30% change in normalized current, 25 ms. Bottom: eIPSC amplitude measured from pairs of neighboring BDNF-KO and BDNF-WT neurons in response to stimulation of

**Figure 19 (Continued)**. axons in (A) radiatum, (B) pyramidale, or (C) oriens. Open circles indicate individual BDNF-KO/BDNF-WT pairs. Red circles indicate the mean ± SEM. Significance was determined by paired two-tailed t-test.

(D-F) eIPSC measured from mice 24 hours post-KA injection. Top: Normalized, average eIPSC measured from BDNF-WT (black) and BDNF-KO (green) neurons in response to stimulation of axons in (D) radiatum, (E) pyramidale, or (F) oriens are shown. Data are shown as the mean (line) ± SEM (shaded region). Scale bars: 30% change in normalized current, 25 ms. Bottom: eIPSC amplitude measured from pairs of neighboring BDNF-KO and BDNF-WT neurons in response to stimulation of axons in (G) radiatum, (H) pyramidale, or (I) oriens. Open circles indicate individual BDNF-KO/BDNF-WT pairs. Red circles indicate the mean ± SEM. Significance was determined by paired two-tailed t-test.

conditional mice ($BDNF^{f/f}$) mice and compared eIPSCs between neighboring BDNF knockout and BDNF wild type neurons (BDNF-KO and BDNF-WT, respectively) in response to stimulation of axons in the somatic layer, apical dendrites or basal dendrites. In mice housed in standard conditions, we found no differences in eIPSC amplitude measured from neighboring BDNF-KO and BDNF-WT neurons upon stimulation of axons in any of the layers of the hippocampus analyzed (**Figure 18**). This indicates that the disruption of BDNF function in the hippocampus of mice housed under standard conditions, where NPAS4 is not expressed, does not have a significant effect on inhibitory synapses that form on pyramidal neurons.

By contrast, when we exposed mice to environmental enrichment to induce NPAS4 as well as BDNF expression and secretion, stimulation of axons in the pyramidal cell layer results in a significant smaller amplitude eIPSC in BDNF-KO neurons relative to neighboring BDNF-WT neurons (**Figure 19**, Supplemental Table 2, $p<0.05$). The disruption of BDNF function did not have a significant effect on eIPSC amplitude when axons in stratum radiatum or oriens were stimulated and the eIPSCs in BDNF-WT and BDNF-KO neurons were compared (**Figure 19**). Similar results were observed when BDNF expression was induced with KA (**Figure 19**). Taken together these findings suggest that the differential effects of NPAS4 on pyramidal neuron inhibition are mediated, at least in part, through the induction of BDNF that functions selectively to promote inhibition at the soma. Given that the disruption of BDNF function does not affect eIPSCs in radiatum or oriens, the effect of NPAS4 on inhibition of CA1 pyramidal

neuron apical dendrites described above is likely mediated by NPAS4 targets other than BDNF.

## Chapter 3: Conclusions and thoughts on the future

**Conclusions and thoughts on the future**

These findings indicate that when a mouse engages with its environment, the neuronal activity-regulated transcription factor NPAS4 is expressed in pyramidal neurons of the hippocampus where it functions to promote inhibitory synapse formation on the cell body and inhibitory synapse destabilization in the apical dendrites. In light of recent reports indicating that inhibition within these cellular domains can have distinct functions, we speculate that this redistribution of inhibition we observe in response to sensory stimulation will have a significant effect on information processing in the postsynaptic neuron. First, the opposing regulation of somatic and apical dendritic inhibition may allow integration or plasticity of excitatory events in the apical dendrites or propagation of dendritic APs while still limiting the generation of somatic APs and thus the propagation of information to downstream neurons. This is in contrast to homeostatic scaling of inhibitory synapses – a process whereby the AP output of a neuron is regulated by cell-wide scaling of synaptic strengths that preserves the relative strengths among synapses. Second, many inhibitory neurons synapse locally on hundreds of pyramidal neurons. Concurrent induction of NPAS4 in multiple pyramidal neurons may coordinate the activity of those neurons by selectively strengthening or weakening a class of common inhibitory inputs. Additionally, several interneuron subtypes generate APs at specific phases of network oscillations or are suppressed during oscillatory activity (Cobb et al., 1995; Fuentealba et al., 2008; Klausberger, 2009; Klausberger et al., 2003; Klausberger et al., 2005). NPAS4 regulation of synapses formed by these neurons may bias a neuron to opt in or out of firing with an existing ensemble of neurons.

Transcriptional regulation of these circuit features may also underlie recent findings that associate NPAS4 function with contextual or stimulus dependent fear conditioning (Ploski et al., 2011; Ramamoorthi et al., 2011).

Identification of the inhibitory neurons that form NPAS4-regulated synapses will be an exciting, and challenging undertaking given the large number of different subtypes of inhibitory neuron that have been identified. Future studies will be necessary to decipher further the NPAS4-dependent gene program and identify additional genes involved in domain-specific regulation of inhibition. Collectively, the expression and action of these genes may contribute to the representation of complex sensory features, execution of elaborate motor programs, or determine how circuits are engaged during learning and memory.

| strain | genotype | stimulus | | mIPSC | | | | | |
|---|---|---|---|---|---|---|---|---|---|
| | | | | frequency (Hz) | | | amplitude (pA) | | |
| | | | n | average | sem | p value | average | sem | p value |
| *Npas4*$^{tf}$ | WT | standard housing | 14 pairs | 6.27 | 0.55 | 0.88 | 40.96 | 1.92 | 0.35 |
| | KO | standard housing | | 6.2 | 0.37 | | 39.1 | 2.12 | |
| *Npas4*$^{tf}$ | WT | EE | 23 pairs | 6.94 | 0.36 | < 0.05 | 38.39 | 1.60 | 0.26 |
| | KO | EE | | 5.70 | 0.63 | | 35.94 | 1.96 | |
| *Npas4*$^{tf}$ | WT | KA | 26 pairs | 5.8 | 0.47 | < 0.01 | 39.74 | 1.11 | < 0.05 |
| | KO | KA | | 3.25 | 0.34 | | 35.07 | 1.72 | |
| C57bl6/J | WT; GFP- | standard housing | 17 pairs | 4.15 | 0.41 | 0.16 | 40.49 | 1.9 | 0.38 |
| | WT; GFP+ | standard housing | | 4.6 | 0.44 | | 42.45 | 1.53 | |
| C57bl6/J | WT; GFP- | KA | 17 pairs | 5.29 | 0.54 | 0.93 | 42.22 | 2.38 | 0.23 |
| | WT; GFP+ | KA | | 5.24 | 0.42 | | 45.48 | 1.7 | |
| EMX-Cre;*Npas4*$^{tf}$ | KO | standard housing | 14 cells | 4.78 | 0.45 | < 0.01 | 42.12 | 0.55 | < 0.05 |
| | KO | KA | 16 cells | 3.05 | 0.25 | | 37.16 | 0.46 | |

**Figure 20. Summary statistics for mIPSC data.**

| eIPSC | | | Lacunosum (pA) | | | | Radiatum (pA) | | | |
|---|---|---|---|---|---|---|---|---|---|---|
| | | | n | average | sem | p value | n | average | sem | p value |
| Npas4$^{lf}$ | WT | standard housing | 14 pairs | 20.98 | 3.60 | 0.65 | 13 pairs | 325.23 | 47.38 | 0.99 |
| | KO | standard housing | | 21.78 | 3.66 | | | 325.63 | 72.00 | |
| Npas4$^{lf}$ | WT | EE | 16 pairs | 31.10 | 4.07 | 0.60 | 16 pairs | 323.26 | 61.64 | < 0.05 |
| | KO | EE | | 29.33 | 3.27 | | | 449.46 | 69.94 | |
| Npas4$^{lf}$ | WT | KA | 13 pairs | 18.92 | 3.21 | 0.92 | 17 pairs | 170.12 | 27.50 | < 0.05 |
| | KO | KA | | 18.65 | 2.56 | | | 255.36 | 38.34 | |
| BDNF$^{lf}$ | WT | standard housing | | n/a | | | 14 pairs | 367.23 | 94.29 | 0.72 |
| | KO | standard housing | | n/a | | | | 353.17 | 100.57 | |
| BDNF$^{lf}$ | WT | EE | | n/a | | | 10 pairs | 262.95 | 48.13 | 0.80 |
| | KO | EE | | n/a | | | | 282.67 | 59.19 | |
| BDNF$^{lf}$ | WT | KA | | n/a | | | 14 pairs | 183.00 | 38.16 | 0.93 |
| | KO | KA | | n/a | | | | 186.12 | 47.67 | |

| | | | Pyramidal (pA) | | | | Oriens (pA) | | | |
|---|---|---|---|---|---|---|---|---|---|---|
| | | | n | average | sem | p value | n | average | sem | p value |
| Npas4$^{lf}$ | WT | standard housing | 17 pairs | 1217.12 | 130.98 | 0.69 | 13 pairs | 414.00 | 117.93 | 0.49 |
| | KO | standard housing | | 1251.15 | 149.37 | | | 385.87 | 111.57 | |
| Npas4$^{lf}$ | WT | EE | 14 pairs | 1610.55 | 178.19 | < 0.01 | 18 pairs | 876.06 | 183.21 | 0.61 |
| | KO | EE | | 1209.48 | 191.04 | | | 833.71 | 182.37 | |
| Npas4$^{lf}$ | WT | KA | 18 pairs | 1032.78 | 152.49 | < 0.01 | 15 pairs | 346.46 | 64.82 | < 0.05 |
| | KO | KA | | 503.38 | 84.61 | | | 208.97 | 44.78 | |
| BDNF$^{lf}$ | WT | standard housing | 15 pairs | 766.37 | 101.41 | 0.33 | 11 pairs | 469.59 | 140.70 | 0.91 |
| | KO | standard housing | | 642.69 | 122.66 | | | 472.80 | 184.51 | |
| BDNF$^{lf}$ | WT | EE | 14 pairs | 805.24 | 493.30 | <0.05 | 14 pairs | 183.00 | 38.16 | 0.93 |
| | KO | EE | | 128.01 | 92.03 | | | 186.12 | 47.67 | |
| BDNF$^{lf}$ | WT | KA | 12 pairs | 1320.23 | 208.21 | < 0.01 | 15 pairs | 592.16 | 114.12 | 0.84 |
| | KO | KA | | 721.82 | 186.43 | | | 572.77 | 136.89 | |

| | | | Lacunosum slope (%max/ms) | | | | Radiatum slope (%max/ms) | | | |
|---|---|---|---|---|---|---|---|---|---|---|
| | | | n | average | sem | p value | n | average | sem | p value |
| Npas4$^{lf}$ | WT | standard housing | 14 pairs | 4.9 | 0.4 | 0.58 | 13 pairs | 23 | 4 | 0.53 |
| | KO | standard housing | | 4.7 | 0.3 | | | 27 | 6 | |
| Npas4$^{lf}$ | WT | EE | 16 pairs | 4.3 | 0.4 | 0.84 | 16 pairs | 15 | 2 | 0.13 |
| | KO | EE | | 4.3 | 0.2 | | | 19 | 4 | |
| Npas4$^{lf}$ | WT | KA | 13 pairs | 4.1 | 0.3 | 0.89 | 17 pairs | 26 | 5 | 0.96 |
| | KO | KA | | 4.2 | 0.3 | | | 26 | 5 | |

| | | | Pyramidal slope (%max/ms) | | | | Oriens slope (%max/ms) | | | |
|---|---|---|---|---|---|---|---|---|---|---|
| | | | n | average | sem | p value | n | average | sem | p value |
| Npas4$^{lf}$ | WT | standard housing | 17 pairs | 42 | 5 | 0.41 | 13 pairs | 25 | 7 | 0.25 |
| | KO | standard housing | | 48 | 6 | | | 33 | 9 | |
| Npas4$^{lf}$ | WT | EE | 14 pairs | 35 | 5 | 0.84 | 18 pairs | 22 | 4 | 0.81 |
| | KO | EE | | 36 | 4 | | | 23 | 4 | |
| Npas4$^{lf}$ | WT | KA | 18 pairs | 47 | 7 | 0.67 | 15 pairs | 29 | 5 | 0.93 |
| | KO | KA | | 44 | 6 | | | 30 | 7 | |

Radiatum $PPR_{Npas4\text{-}WT}/PPR_{Npas4\text{-}KO}$

| | | | n | Isi 25 | Isi 50 | Isi 100 | Isi 200 | p value |
|---|---|---|---|---|---|---|---|---|
| Npas4$^{lf}$ | WT | standard housing | 9 pairs | 1.10 ± 0.11 | 1.08 ± 0.15 | 1.13 ± 0.10 | 0.955 ± 0.11 | > 0.05 |
| | KO | standard housing | | | | | | |
| Npas4$^{lf}$ | WT | EE | 16 pairs | 1.06 ± 0.12 | 1.04 ± 0.09 | 1.04 ± 0.14 | 1.24 ± 0.18 | > 0.05 |
| | KO | EE | | | | | | |
| Npas4$^{lf}$ | WT | KA | 11 pairs | 1.31 ± 0.25 | 1.06 ± 0.11 | 1.03 ± 0.11 | 0.95 ± 0.06 | > 0.05 |
| | KO | KA | | | | | | |

Pyramidal $PPR_{Npas4\text{-}WT}/PPR_{Npas4\text{-}KO}$

| | | | n | Isi 25 | Isi 50 | Isi 100 | Isi 200 | p value |
|---|---|---|---|---|---|---|---|---|
| Npas4$^{lf}$ | WT | standard housing | 10 pair | 1.03 ± 0.12 | 0.89 ± 0.087 | 1.06 ± 0.12 | 1.09 ± 0.073 | > 0.05 |
| | KO | standard housing | | | | | | |
| Npas4$^{lf}$ | WT | EE | 11 pairs | 1.18 ± 0.19 | 1.03 ± 0.10 | 1.03 ± 0.13 | 1.08 ± 0.11 | > 0.05 |
| | KO | EE | | | | | | |
| Npas4$^{lf}$ | WT | KA | 13 pairs | 1.25 ± 0.25 | 1.01 ± 0.10 | 0.97 ± 0.079 | 1.06 ± 0.059 | > 0.05 |
| | KO | KA | | | | | | |

Oriens $PPR_{Npas4\text{-}WT}/PPR_{Npas4\text{-}KO}$

| | | | n | Isi 25 | Isi 50 | Isi 100 | Isi 200 | p value |
|---|---|---|---|---|---|---|---|---|
| Npas4$^{lf}$ | WT | standard housing | 8 pairs | 1.13 ± 0.22 | 1.05 ± 0.13 | 1.02 ± 0.10 | 1.03 ± 0.10 | > 0.05 |
| | KO | standard housing | | | | | | |
| Npas4$^{lf}$ | WT | EE | 16 pairs | 1.32 ± 0.20 | 1.05 ± 0.10 | 0.92 ± 0.08 | 1.05 ± 0.11 | > 0.05 |
| | KO | EE | | | | | | |
| Npas4$^{lf}$ | WT | KA | 8 pairs | 0.85 ± 0.19 | 0.95 ± 0.21 | 0.99 ± 0.17 | 0.89 ± 0.11 | > 0.05 |
| | KO | KA | | | | | | |

**Figure 21. Summary statistics for eIPSC data.**

| genotype | stimulus | layer | capacitance (pF) | | input resistance (MΩ) | | series resistance (MΩ) | |
|---|---|---|---|---|---|---|---|---|
| | | | average | sem | average | sem | average | sem |
| WT | standard housing | n/a | 86.63 | 16.43 | 180.56 | 11.97 | 19.78 | 0.61 |
| KO | standard housing | n/a | 101.42 | 12.99 | 171.99 | 11.76 | 19.07 | 0.88 |
| WT | EE | n/a | 97.46 | 9.56 | 181.92 | 12.34 | 19.29 | 0.78 |
| KO | EE | n/a | 93.05 | 9.87 | 177.41 | 12.45 | 19.19 | 0.83 |
| WT | KA | n/a | 72.10 | 8.33 | 216.20 | 13.10 | 17.78 | 0.79 |
| KO | KA | n/a | 57.55 | 5.09 | 218.17 | 11.22 | 19.33 | 0.60 |
| WT; GFP- | standard housing | n/a | 71.61 | 9.40 | 171.45 | 9.12 | 19.27 | 0.80 |
| WT; GFP+ | standard housing | n/a | 95.54 | 13.07 | 160.64 | 11.44 | 19.78 | 0.70 |
| WT; GFP- | KA | n/a | 77.17 | 7.11 | 197.35 | 9.38 | 19.73 | 0.87 |
| WT; GFP+ | KA | n/a | 83.38 | 7.84 | 188.56 | 13.41 | 19.37 | 0.80 |
| KO | standard housing | n/a | *37.23 | 3.24 | 278.94 | 15.41 | 19.28 | 0.78 |
| KO | KA | n/a | *51.31 | 4.94 | 240.13 | 20.05 | 18.72 | 0.90 |
| WT | standard housing | lacunosum | 46.48 | 4.28 | 267.91 | 24.08 | 22.95 | 1.42 |
| KO | standard housing | lacunosum | 51.21 | 4.86 | 275.47 | 25.59 | 22.12 | 1.07 |
| WT | standard housing | radiatum | 76.66 | 9.44 | 267.68 | 44.28 | 19.58 | 0.96 |
| KO | standard housing | radiatum | 77.23 | 10.91 | 260.23 | 28.09 | 20.95 | 1.04 |
| WT | standard housing | pyramidal | 66.67 | 11.09 | 296.67 | 40.43 | 18.94 | 1.03 |
| KO | standard housing | pyramidal | 80.22 | 15.55 | 278.97 | 33.60 | 18.21 | 1.05 |
| WT | standard housing | oriens | 56.04 | 8.39 | 252.44 | 30.09 | *17.92 | 0.93 |
| KO | standard housing | oriens | 62.11 | 12.87 | 219.38 | 22.84 | *19.39 | 1.05 |
| WT | EE | lacunosum | 76.70 | 8.03 | 314.64 | 26.25 | 19.76 | 0.82 |
| KO | EE | lacunosum | 61.66 | 7.72 | 273.70 | 21.45 | 19.84 | 1.03 |
| WT | EE | radiatum | 83.22 | 11.30 | 286.41 | 21.93 | 18.95 | 0.93 |
| KO | EE | radiatum | 89.71 | 12.41 | 293.39 | 29.71 | 18.43 | 0.96 |
| WT | EE | pyramidal | 97.04 | 13.37 | 331.76 | 27.51 | 19.44 | 0.93 |
| KO | EE | pyramidal | 82.09 | 11.35 | 297.26 | 16.24 | 18.79 | 0.80 |
| WT | EE | oriens | 85.25 | 12.37 | 225.53 | 29.39 | 18.94 | 0.92 |
| KO | EE | oriens | 86.69 | 13.91 | 248.42 | 39.46 | 18.76 | 0.76 |
| WT | KA | lacunosum | 82.19 | 14.09 | 361.75 | 56.95 | 23.48 | 1.91 |
| KO | KA | lacunosum | 66.50 | 15.16 | 290.86 | 37.19 | 24.28 | 1.70 |
| WT | KA | radiatum | 79.96 | 9.56 | 232.94 | 21.21 | 21.47 | 1.18 |
| KO | KA | radiatum | 91.90 | 9.16 | 246.18 | 21.50 | 21.50 | 1.06 |
| WT | KA | pyramidal | 71.39 | 7.33 | 288.68 | 50.36 | 22.95 | 1.00 |
| KO | KA | pyramidal | 65.51 | 11.14 | 242.72 | 22.71 | 22.81 | 1.25 |
| WT | KA | oriens | 79.93 | 10.95 | 223.81 | 19.93 | 20.87 | 0.81 |
| KO | KA | oriens | 103.04 | 15.72 | 245.35 | 49.69 | 21.00 | 1.20 |
| WT | standard housing | radiatum | 55.64 | 9.37 | 409.04 | 37.02 | 19.14 | 0.57 |
| KO | standard housing | radiatum | 52.50 | 8.92 | 363.68 | 45.34 | 20.11 | 0.49 |
| WT | standard housing | pyramidal | 73.47 | 10.20 | 401.44 | 28.41 | 20.19 | 0.83 |
| KO | standard housing | pyramidal | 56.93 | 11.15 | 340.33 | 32.63 | 20.46 | 0.94 |
| WT | standard housing | oriens | 65.00 | 8.84 | 275.87 | 45.71 | 19.08 | 1.01 |
| KO | standard housing | oriens | 65.53 | 13.07 | 288.82 | 48.97 | 19.82 | 0.78 |
| WT | KA | radiatum | 39.43 | 6.26 | 394.16 | 22.47 | 20.93 | 0.75 |
| KO | KA | radiatum | 42.49 | 6.09 | 371.60 | 23.43 | 20.82 | 0.64 |
| WT | KA | pyramidal | 44.26 | 8.88 | 446.55 | 29.44 | 20.15 | 0.89 |
| KO | KA | pyramidal | 44.30 | 8.24 | 385.21 | 28.96 | 20.50 | 0.80 |
| WT | KA | oriens | 44.93 | 8.50 | 414.02 | 83.26 | 18.77 | 0.65 |
| KO | KA | oriens | 46.08 | 6.73 | 399.29 | 94.40 | 19.11 | 0.78 |

**Figure 22. Summary statistics for membrane properties.**

# Chapter 4: Experimental procedures

**Animal husbandry and handling**

Animals were handled according to protocols approved by the Harvard University Standing Committee on Animal Care and the University of California San Diego Institutional Animal Care and Use Committee, and were in accordance with federal guidelines.

For experiments in which mice were exposed to an enriched environment, three days after virus injection (postnatal day 16-18, p16-18) animals were moved to a larger cage that contained a running wheel, hut, tunnel, and several other novel objects. To maximize novelty, the objects in the environment were rearranged and new objects introduced every second day. Mice were housed in the enriched environment for 4-10 days. Although we detect a limited number of NPAS4 positive excitatory neurons at a given time point, exploration of a novel environment increases NPAS4 immunoreactivity to an extent similar to that observed for other activity inducible genes such as Fos and Arc. Moreover, behaviorally triggered NPAS4 induction appears to occur iteratively, and in distinct subpopulations of neurons as the animal engages and explores novel features of the environment, such that the number of NPAS4 immuno-positive neurons detected at any given time point significantly underestimates the number of neurons that express NPAS4 over a period of several days.

For experiments in which seizures were induced, intraperitoneal injection of kainic acid (2.5-10 mg/kg) was used. In this paradigm, mice were sacrificed at 3 hours

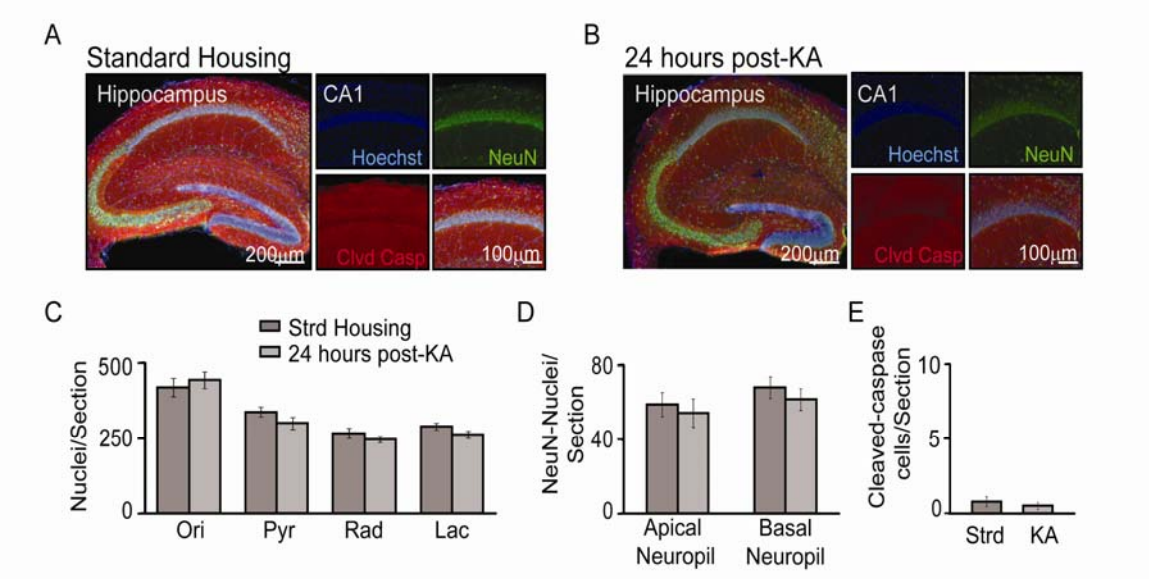


**Figure 23. Kainic acid does not induce cell death within 24 hours.**

(A-B) Representative hippocampal sections from a mouse housed under (A) standard conditions or (B) 24 hours post-KA injection. Sections were immunostained for NeuN (green) and Cleaved-Caspase 3 (red) and counterstained with Hoechst (blue).

(C-E) Quantification of (C) Hoechst+ nuclei, (D) NeuN+ nuclei, and (E) Cleaved-caspase+ cells per 40um section of hippocampus in all layers of the hippocampus. Data are shown as mean ± SEM.

(immunohistochemistry) or 24 hours (electrophysiology) post-kainic acid injection. Electrophysiology experiments were done 24 hours after KA injection to allow sufficient time for NPAS4 induction, the execution of an NPAS4-dependent program of gene expression, and potential synaptic regulation but before detectable seizure related cell death (**Figure 23**).

**Sterotaxically guided surgery**

All surgeries were performed according to protocols approved by the Harvard University Standing Committee on Animal Care and the University of California San Diego Institutional Animal Care and Use Committee, and were in accordance with federal guidelines. Surgeries were performed on mice between P13 and P15. Animals were deeply anesthetized by inhalation of isoflurane (initially 3-5% in $O_2$, maintained with 1-2%) and secured in the stereotaxic apparatus (Kopf). The fur was shaved and scalp cleaned with betadine and 100% ethanol three times before an incision was made to expose the skull. A small hole was drilled through the skull and the CA1 region of hippocampus was specifically targeted for injection (medial/lateral: ± 2.9mm, anterior/posterior: -2.5mm, dorsal/ventral: 2.8mm below the dura). An injection needle (Drummond Wiretrol® II) was gradually lowered to the appropriate depth, the tissue allowed to settle, and the virus injected (250-300nL; 150nL/min). Five minutes post-injection, the needle was retracted, the scalp sutured, and the mouse returned to its home cage. All animals were monitored for at least one hour post-surgery and at 12 hour intervals for the next 5 days. Postoperatively, analgesic (flunixin, 2.5mg/Kg) was

administered at 12 hour intervals for 72 hours.

**Virus production**

AAV-Cre-GFP was produced by the Harvard Gene Therapy Initiative or UNC Vector Core with a plasmid provided by Matthew During (Ohio State University). The plasmids containing the genome for AAV-EF1a-YFP-2A-Cre, AAV-mCherrey-IRES-Cre, and AAV-dfi-GFP-gephyrin were generated using standard molecular cloning techniques and were produced by the UNC Vector Core.

**Acute slice preparation**

Transverse hippocampal slices were prepared from Npas4$^{f/f}$, EMX-Cre;NPAS4$^{f/f}$, BDNF$^{f/f}$ or C57Bl/6 mice (P21-27). Animals were anesthetized by inhalation of isoflurane. The cerebral hemispheres were quickly removed and placed into ice-cold choline-based artificial cerebrospinal fluid (choline-ACSF) consisting of (in mM): 110 Choline-Cl, 25 $NaHCO_3$, 1.25 $Na_2HPO_4$, 2.5 KCl, 7 MgCl, 25 glucose, 0.5 $CaCl_2$, 11.6 ascorbic acid, 3.1 pyruvic acid and equilibrated with 95% $O_2$/5% $CO_2$. Tissue was blocked and transferred to a slicing chamber containing choline-ACSF. Slices (300μm) were cut with a LeicaVT1000s vibratome (Leica Instruments, Nussloch, Germany) and transferred to a holding chamber containing ACSF consisting of (in mM): 127 NaCl, 25 $NaHCO_3$, 1.25 $Na_2HPO_4$, 2.5 KCl, 2 $CaCl_2$, 1 $MgCl_2$, 25 glucose, and saturated with 95% $O_2$/5% $CO_2$. Slices were incubated at 30°C for 30-40 minutes and then kept at room temperature for no more than 6 hours until recordings were performed. For mice injected with AAV-Cre-

GFP, slices showing infection of between 20-40% in CA1, as determined by GFP fluorescence, were used for recording. Slices showing greater than ~40% infected neurons or infection outside of CA1 were discarded.

**Organotypic Slice preparation and transfection**

Organotypic hippocampal slices were prepared as previously described [45]. Briefly, hippocampi were rapidly dissected from wild type mice at P7 in ice cold dissection media consisting of (in mM): 1 $CaCl_2$, 5 $MgCl_2$, 10 glucose, 4 KCl, 26 $NaHCO_3$, 218 sucrose, 1.3 $NaH_2PO_4 \cdot H_2O$, 30 HEPES. Tissue was transferred to a tissue chopper (McIlwan Ted Pella, Inc) and 400um thick sections cut. Sections were transferred to tissue culture plates and grown on PTFE inserts (Milicell Organotypic insert, EMD Millipore) in slice culture media consisting of (in mM or percent) 1X MEM, 20% horse serum, 1 L-glutamine, 0.125% ascorbic acid, 1 $CaCl_2$, 2 $MgCl_2$, 12.8 glucose, 5.25 $NaHCO_3$, 30 HEPES, pH 7.4, 320 mOsm) for 7-10 days. On the second day in vitro, cultures were biolistically (Gene Gun, Biorad) co-transfected with 1μm gold particles coated with GFP and shRNAs targeting the gene of interest (particles prepared with GFP 15 μg, 3-9 μg of shRNA, pcDNA3 to a final DNA mass of 50 μg per the manufacturer's instructions). shRNA sequences are included in the Figure 25.

**Electrophysiology**

Whole-cell voltage clamp recordings were obtained from CA1 pyramidal neurons visualized under IR-DIC. Neurons were held at -70mV except for experiments measuring

evoked responses from stimulation of axons in stratum lacunosum-moleculare, during which neurons were held at 0 mV (see below). Patch pipettes (open pipette resistance 2-4 MOhms) were filled with an internal solution consisting of (in mM) 147 CsCl, 5 $Na_2$-phosphocreatine, 10 HEPES, 2 MgATP, 0.3 $Na_2$GTP and 2 EGTA. Osmolarity and pH were adjusted to 300 mOsm and 7.3 with double distilled water and CsOH, respectively. In experiments where mIPSCs recorded, currents were pharmacologically isolated with bath application of 0.5μM tetrodotoxin citrate (Tocris Bioscience), 10 μM (R)-CPP (Tocris Bioscience), 10 μM NBQX disodium salt (Tocris Bioscience) to antagonize voltage gated sodium channels, GluN receptors, and GluA receptors, respectively. In experiments where eIPSCs were recorded, inhibitory currents were pharmacologically isolated with bath application of CPP and NBQX. Additionally, 5 mM QX-314 (Sigma) was added to the internal solution to antagonize voltage gated sodium channels in the patched neuron. Extracellular stimulation of local axons within specific lamina of the hippocampus was delivered by current injection through a theta glass stimulating electrode, to restrict the spatial extent of stimulation, that was placed in the center of the relevant layer (along the somato-dendritic axis of the CA1 neuron) and within 100-200 μm laterally of the patched pair. The stimulus strength was the minimum required to generate an eIPSC in both NPAS4-KO and NPAS4-WT neurons.

When postsynaptic neurons were held at -70mV, no eIPSC was observed in response to stimulation of axons in lacunosum-molecular. This is likely because eIPSCs originating in lacunosum-molecular are extensively filtered by the dendrites, the somatic patch pipet

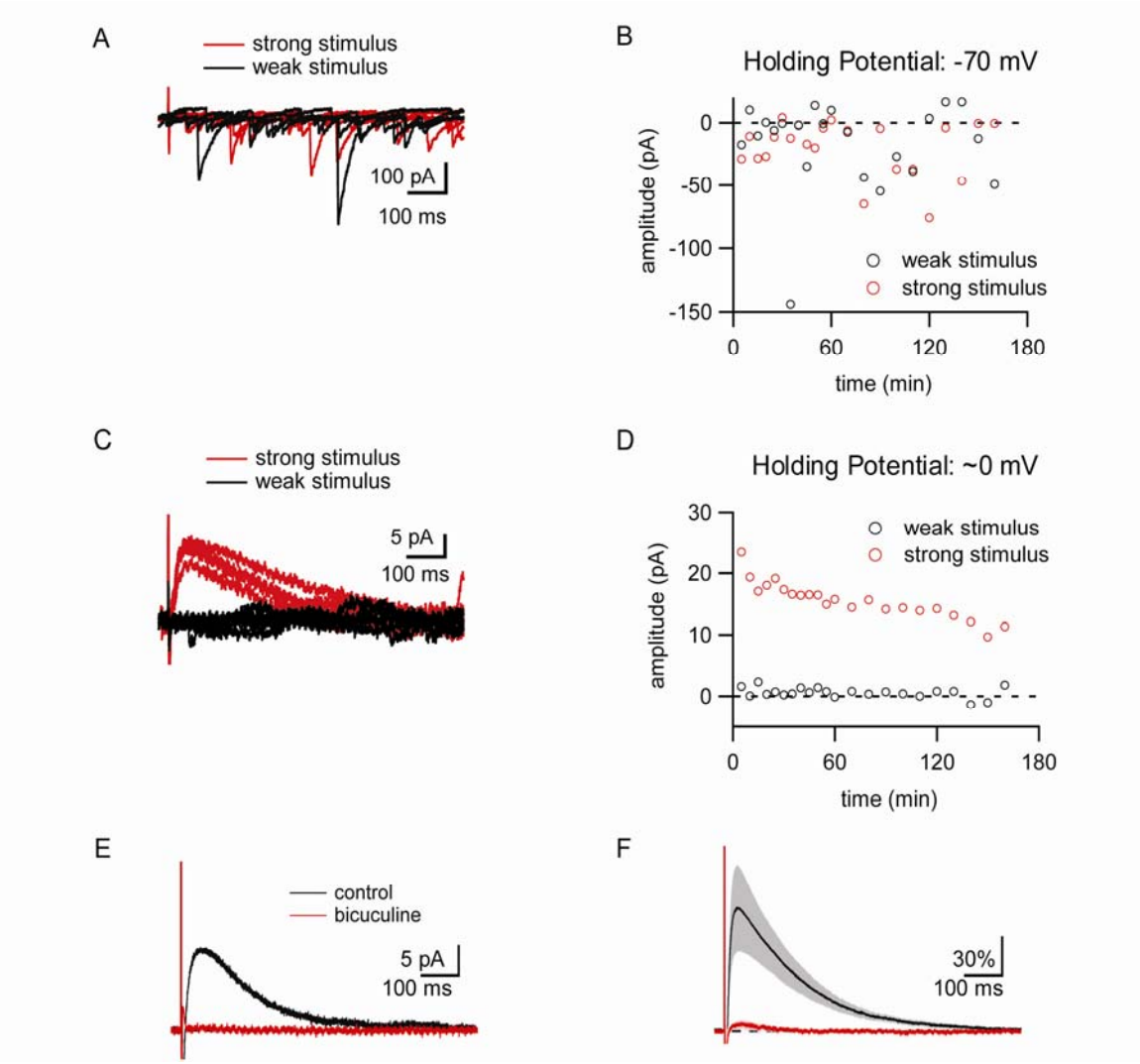


**Figure 24. Measuring eIPSCs from stimulation of axons in lacunosum-moleculare.**

(A) Example current recordings in response to weak (10 μA, black) and strong (100 μA, red) extracellular stimulation of axons in lacunosum-moleculare. This cell is summarized in (B, D). Vclamp = -70, 30 minutes post-break in. Many large spontaneous IPSCs are seen throughout the recordings.

(B) Summary of eIPSCs measured in response to weak (black) and strong (red) extracellular stimulation of axons in lacunosum-moleculare. Vclamp = -70 mV. The

strong and weak extracellular stimuli are indistinguishable in part because the evoked eIPSCs are overwhelmed by spontaneous events occurring throughout the neuron.

**Figure 24 (Continued)**. (C) Example current recordings in response to weak (black) and strong (red) extracellular stimulation of axons in lacunosum-moleculare from the cell summarized in (B, D). Vclamp = 0 mV, 30 minutes post-break in. Holding the neuron at 0mV (~ECl) reduces the appearance of spontaneous IPSCs that are generated by proximal inhibitory synapses. At this membrane potential, stimulation of axons in lacunosum-moleculare generates a small, slow, outward current. This suggests that dendrites in lacunosum-moleculare are sufficiently distal from the patch pipette that we are unable to clamp their membrane potential and that the chloride concentration does not equilibrate with that of the intracellular recording solution.

(D) Summary of eIPSCs measured in response to weak (black) and strong (red) extracellular stimulation of axons in lacunosum-moleculare. Vclamp = 0 mV. The strong and the weak extracellular stimuli are clearly distinguishable as failures and successes and peak eIPSCs are time-locked to the stimulus.

(E) Example of an eIPSC generated in response to stimulation of axons in lacunosum-moleculare before (black) and after (red) wash in of the GABAA/CR antagonist bicuculline.

(F) Summary data of eIPSCs generated in response to stimulation of axons in lacunosum-moleculare before (black) and after (red) wash in of the GABAA/cR antagonist bicuculline. n = 4. Data are shown as the mean (line) ± SEM (shaded region).

| | | |
|---|---|---|
| **NPAS4** | **Iqsec3** | **Fer1l3** |
| shRNA1 GAAACAAACTGGTGCTTAT | shRNA1 CCACAGACACCCTGCGCAA | shRNA1 CAAATATAATTGAGCGGAA |
| shRNA2 GGCTGAAAGTGGAGATATT | shRNA2 CCTCAGGGTCACAGCGGTA | shRNA2 GTGCAGTATTTGACGGGAA |
| shRNA3 ACACAGAGAAAGAGCAAAA | shRNA3 GCAAGAGAGTGGCGCGTAC | shRNA3 GGAAGAAGATCAAGGAGAT |
| **BDNF** | **Pam** | **Cpa4** |
| shRNA1 GGTCACAGTCCTAGAGAAA | shRNA1 GCATTGAGGTCCCGGAAAT | shRNA1 GGATATGTGTACACGCAAA |
| shRNA2 TCTTTCTGCTGGAGGAATA | shRNA2 CTAAAGAGTCTGACACGTA | shRNA2 TGGACGATGTGGCGAGGAA |
| shRNA3 GTATGTACACTGACCATTA | shRNA3 CCTATTGATTCTTCGGATT | shRNA3 CCATCTGGACAGCGAGGAA |
| **Cyr61** | **Slc6a17** | **Tll1** |
| shRNA1 AGGTGGAGTTAACGAGAAA | shRNA1 GCAATGAGCATGTCACCGA | shRNA1 GGTTGGTGGTCTCGGGTAT |
| shRNA2 CTGTAAGGTCTGCGCTAAA | shRNA2 CCAATCTGGAGGAGAACGA | shRNA2 GTGCAAAGCTGCTGTGTTT |
| shRNA3 GGTGAAAGTCAGCGGGCAG | shRNA3 GGGCATGGCTGTCGTCAAG | shRNA3 TGAGAGAAGTGATGAAGAA |
| **Pcsk1** | **Rgs2** | **Kcnj3** |
| shRNA1 GCTGAAAGGGAAAGAGATA | shRNA1 ACATAGACTTCCAAACGAA | shRNA1 CCATGAAACTCCAACGAAT |
| shRNA2 CCAGAAGGCATTTGAATAT | shRNA2 GGTTCTTGGAGTCCGAATT | shRNA2 CCTCATGTTTAGCGAGCAT |
| shRNA3 GAAGAAAGAATGTGTTGTA | shRNA3 GGACAAGAGTGCAGGCAAC | shRNA3 AGAAGAAACGGCAGCGGTT |
| **Nptx2** | **Auh** | **Dbc1** |
| shRNA1 CGGGCAAGCCAACGAGATT | shRNA1 GCATTGTGGTGCTCGGGAT | shRNA1 CGGCAAGGATTTACAACCA |
| shRNA2 GCAAGGACACCATGGGCGA | shRNA2 GGTGGATGCATTAAAGTCA | shRNA2 GCAATCAAGGTCACAGAAA |
| shRNA3 AGACAGAGAGCACGCTGAA | shRNA3 CCTCAAGATGTTATCAAAA | shRNA3 GAGAGGAGGCTTTGACCAT |
| **Dkk2** | **Nfil3** | **Nr4a3** |
| shRNA1 CTGGATGGCACCCGGCATA | shRNA1 CCGCACAAGCTTCGGATTA | shRNA1 GGAAGAGGGTCGCGAGCAT |
| shRNA2 CCAAGATGCCTCATATAAA | shRNA2 TGGGAGAAACGGCGGAAAA | shRNA2 CCAAAGAAGATCAGACGTT |
| shRNA3 GGAATGTGAAGTTGGAAGA | shRNA3 TCTCAGTGCAGGTGACGAA | shRNA3 AGACTTATGGCTCGGAATA |
| **Fosl2** | **cFos** | **Dusp6** |
| shRNA1 CTGCAGTCCTTGCGCGGTA | shRNA1 GAGGAAGAGAAACGGAGAA | shRNA1 GAACGATGCTTACGACATT |
| shRNA2 GAGGAGGAGAAGCGTCGAA | shRNA2 CGGGAATGGTGAAGACCGT | shRNA2 GTGCCAAGGACTCGACCAA |
| shRNA3 GTGATCAAGACCATCGGTA | shRNA3 CTGCTGAAAGAGAAGGAAA | shRNA3 GCAAATTCCTATCTCGGAT |
| **Penk1** | **Per1** | **Hdac9** |
| shRNA1 GGGAGACAACCGTGCGAAA | shRNA1 CCAATAAGGCAGAGAGCGT | shRNA1 GAACAAACTGCTATCGAAA |
| shRNA2 GAAGAAGATGGACGAGCTA | shRNA2 GAGCATATCACATCCGAAT | shRNA2 GCTGGGAATGTGACCGAAA |
| shRNA3 CGATGAAGAAGGCGAAAAT | shRNA3 CCAGTACAACCAAGCGTAA | shRNA3 GCACAGAGGTTAAGCAGAA |
| **Adcyap1** | **Vgf** | **Gpr3** |
| shRNA1 CTTACGACCAGGACGGAAA | shRNA1 AGGAGAAACGGAAGCGGAA | shRNA1 CCATTACCGTTGACCGCTA |
| shRNA2 CCACGAAATCCTTAACGAA | shRNA2 GGGAGGAGGATGACGACGA | shRNA2 GCTTGATGCTGGTCGGCGT |
| shRNA3 GCTACAGCCGCTACCGAAA | shRNA3 GCCAAAGGATGACGGCGTA | shRNA3 TCATCTACGCCTTTCGCAA |
| **FosB** | **Sorcs3** | **Nr4a1** |
| shRNA1 CCGCTAAGGAAGACGGCTT | shRNA1 GGACTGAAGCTGCGGGAAT | shRNA1 GGAAGGAAGATGCCGGTGA |
| shRNA2 TGATCAGCTTGAAGAGGAA | shRNA2 GGTAACAATAGGTGGACGA | shRNA2 GCACATGGCTACCGTGGCA |
| shRNA3 CCTTATGACATGCCAGGAA | shRNA3 GAACTCTCCTATACGGATA | shRNA3 CCGTGACACTTCCGGCATT |
| **JunB** | | |
| shRNA1 GCATCAAAGTGGAGCGAAA | | |
| shRNA2 CCACGGAACTGGAGCGCTT | | |
| shRNA3 GCAGCTACTTTTCGGGTCA | | |

**Figure 25. shRNA sequences used in the screen to identify putative Npas4 target**

**Figure 25 (Continued)**. **genes.**

is unable to clamp the distal dendrites, chloride is continuously extruded along the length of the dendrites and there are a large number of spontaneous IPSCs originating from more proximal parts of the neuron that clutter the recording. By changing the holding potential to 0mV we effectively remove spontaneous IPSCs generated at proximal synapses from the recording revealing a slow outward current in response to stimulation of the axons in lacunosum-molecular that is antagonized by bath application of 50 μM bicuculine methiodide (Sigma, **Figure 24**). Nonetheless, the failure to observe an NPAS4-dependent phenotype in response to stimulation of axons in lacunosum-molecular may reflect a technical limitation of the recording configuration and we cannot exclude the possibility that alterations to inhibitory synapses in this region escape our detection.

**Data Acquisition and Analysis**

Experiments were discarded if the holding current was greater than -500 pA or if the series resistance was greater than 25 MOhms. In experiments where direct comparisons were made between two neurons, recordings were discarded if the series resistance differed by more than 25% between the two recordings. All recordings were performed at room temperature (~20-22°C). Electrophysiology data acquired using pClamp software, either a Multiclamp 700B or Axoclamp 200B amplifier, and digitized with a DigiData 1440 data acquisition board (Axon Instruments, Union City, CA). Data were filtered at 4 or 6 kHz except for experiments with stimulation of axons in lacunosum-moleculare which were filtered at 1 kHz and sampled at 10 kHz. Off-line data analysis was performed using custom software written in Igor Pro (Wavemetrics).

Threshold for mIPSC detection was determined independently for each neuron and was based on the average root mean square (RMS) of that recording (over a 150 ms stretch of the recording that was devoid of clear mIPSCs). Amplitude threshold was set to 1.5 times the average RMS for that cell and recordings were discarded if the RMS was greater than 6 pA. The amplitude of eIPSCs was calculated by averaging the amplitude 0.5 ms before to 2 ms after the peak of the current. Data are shown as positive values for clarity. Slopes of the rise times of the eIPSCs were measured by first normalizing the acquisition to the peak of the eIPSC then measuring the slope between 10-90% of the normalized peak. Paired pulse ratios (PPR) were calculated by recording a template eIPSC for each cell, subtracting the template wave from the first pulse, and then measuring the corrected amplitude of the second peak. Data are shown as the ratio of $PPR_{NPAS4\text{-}WT}/PPR_{NPAS4\text{-}KO}$ to highlight the difference in the PPR at each inter-stimulus interval. Significance was determined by paired two-tailed t-test for direct comparisons of neighboring neurons, two-tailed t-test for comparisons between populations, and one-way ANOVA (Dunnett's test) for PPRs.

**Immunohistochemistry, Sholl analysis, and GFP-gephyrin quantification**

Animals were anesthetized by inhalation of isoflurane. Hippocampi were rapidly dissected in ice cold dissection media as described above and drop fixed in 4% paraformaldehyde in PBS at 4°C for 1.5-3 hours followed by overnight incubation in 30% sucrose in PBS. Cryoprotected tissue was stored in Tissue-Tec O.C.T at -80°C and

subsequently sectioned at a thickness of 40-45 μm (Leica CM1950 cryostat) for immunostaining or GFP-gephryin puncta quantification, or at a thickness of 100 μm for Sholl analysis (Leica Instruments, Nussloch, Germany).

For NPAS4 or cleaved-caspase immunostaining, hippocampal sections were blocked in 2% goat serum and 0.2% Triton X-100 in PBS for 1 hour at room temperature. Sections were incubated in primary antibody overnight at 4°C, washed three times in PBS, incubated in species-matched fluorescently conjugated secondary for 1 hour at room temperature, and again washed in PBS. Finally, sections were mounted on slides with Fluoromount-G (SouthernBiotech). The following antibodies were used: rabbit anti-NPAS4 (1:1000, made in house), mouse anti-NeuN (1:1000, Millipore), rabbit anti-GFP (1:500, Invitrogen), and rabbit anti-Cleaved-Caspase 3 (1:1000, Cell Signaling). The secondary antibodies were Alexa-488 or 555 against the appropriate species (1:500, Invitrogen). When necessary, nuclei were labeled by adding Hoechst 33582 dye (Invitrogen) to the final PBS was at 1:5000. Nuclei positive for the relevant marker were counted and quantified using ImageJ. In $Npas4^{f/f}$ mice that have been sparsely infected with AAV-Cre-GFP and then administered KA, we see dendritic NPAS4 immunoreactivity in the NPAS4-WT but not in the NPAS4-KO neurons. This indicates to us that the low levels of dendritic staining our antibody against NPAS4 generates is likely not a consequence of cross reactivity with another protein.

The neurons used for Sholl analysis were from animals injected with the AAV-EF1a-

YFP-2A-Cre. Neurons imaged for subsequent analysis were infected neurons without other infected neurons nearby to facilitate reconstruction of dendritic morphology. After imaging, the neurons were traced and skeletonized using the NeuronJ plugin for ImageJ and Sholl intersections were subsequently quantified and significance determined by ANOVA.

The neurons used for GFP-gephyrin pucta quantification were from animals injected with AAV-mCherry-IRES-Cre and AAV-dfi-GFP-gephyrin. Few neurons were co-infected likely because of the large size of the GFP-gephyrin insert relative to the capacity of AAV. GFP was not amplified by immunostaining. Sections were images on a Leica SP5 using the resonance scanner. Puncta were called using particle analysis and dendrites/soma traced in ImageJ. Significance was determined by ANOVA.

**Chromatin Immunoprecipitation**

Hippocampi from wild type mice maintained in standard housing or injected with kainic acid (2.5-10 mg/kg, 2-3 hours prior) were rapidly dissected in ice cold dissection media (as above). The tissue was homogenized and DNA and protein were cross linked for 11 minutes (in mM: 10 HEPES-NaOH pH 7.5, 100 NaCl., 1 EDTA. 1 EGTA, 1% formaldehyde, in PBS). Formaldehyde was quenched with 2M glycine in PBS and the sample incubated on a rocker at room temperature for 5 minutes. Tissue was pelleted (200RMP, 5 min, 4˚C), washed with PBS + PMSF, and re-pelleted (2000RPM, 5min, 4˚C). The supernatant was removed and the pellet resuspended in 5ml L1 buffer (in mM:

50 HEPES-NaOH 7.5, 140 NaCl, 1 EDTA, 1EGTA, 0.25% Triton X-100, 0.5% NP40, 10% glycerol, 1M BGP, 0.2M $NaVO_4$, 0.5M NaF, 1X complete protease inhibitor cocktail w/o EDTA (Roche)). The sample was the further homogenized by ten strokes with a tight pestle in a Dounce homogenizer, pelleted (2000RPM, 5min, 4˚C), washed in L1, pelleted and then resuspended in buffer L2 (in mM: 10 Tris-HCl pH 8.0, 100 NaCl, 1M BGP, 0.2M $NaVO_4$, 0.5M NaF, 1X complete protease inhibitor cocktail w/o EDTA (Roche)). Samples were placed on a rotator at room temperature for 10 minutes, pelleted and resuspended in L3 buffer (in mM 10 Tris-HCl pH 8.0, 1 EDTA, 1EGTA, 1M BGP, 0.2M $NaVO_4$, 0.5M NaF, 1X complete protease inhibitor cocktail w/o EDTA (Roche)) to a final concentration of 10M nuclei per mL. Twenty million nuclei were sonicated using a Misonix 3000 for a total time of 7 min, power 7.5, 4˚C). NPAS4 immunoprecipitation was done using protein G Dyna Beads (Life Technologies) according to the manufacturer's instructions using 4 ug of NPAS4 antibody. NPAS4-bound DNA was quantified using qPCR.

**Quantitative PCR**

qPCR of the NPAS4 ChIP DNA was done using the following primer sequences:

us: TGGTGAAAACACTTGGGCATA

TGATGAGCTGGGAACTCTGC

P1: GTCCGCTGGAGACCCTTAGT

CTGAGCCAGTTACGTGACCA

I3: CTTCCCAGATGGTGCTGT

AATCTCCCAGTTCTGCGTTC

P4: CCCTGGAACGGAATTCTTCT

TGCACGAATTACCAGAATCA

Neg1: CATTCAGCACCTTGGACAGA

GCTTGACAGCGAGGAAAAGA

Neg2: GGCCTGAAGTTCAAGGATGG

GCCTGCCACTGAAGCTTGTA

qPCR of the various BDNF isoforms, NPAS4, PCSK1, Adcyap1, and PENK1 were done using the following primer sequences:

Exon1:CACTGAGCAAAGCCGAACTTCTC

TCACCTGGTGGAACATTGTGGC

Exon 2: AGCGGTGTAGGCTGGAATAGACTC

GGTGGAACTTCTTTGCGGCTTAC

Exon 3: TACCCCTTTCTATCATCCCTCCCCG

GAAGCATCCGGCCCGACAGTTCCAC

Exon 4: CGCCATGCAATTTCCACTATCAATAATTTAAC

CGCCTTCATGCAACCGAAGTATG

Exon 5: CCATAACCCCGCACACTCTGTGTAG

CTTCCCGCACCTTCACAGTTCCAC

Exon 6: GATCCGAGAGCTTTGTGTGGAC

GCCTTCATGCAACCGAAGTATG

Exon 7: GGTCCAAGGTCAACGTTTA

TAAACGTTGACCTTGGACC

Exon8: GAACAAACTGATTGCTGAA

TTCAGCAATCAGTTTGTTC

Exon9/coding exon: GATGCCGCAAACATGTCTATGA

TAATACTGTCACACACGCTCAGCTC

NPAS4: AGGGTTTGCTGATGAGTTGC

CCCCTCCACTTCCATCTTC

PCSK1: TGGAGTTGCATATAATTCCAAAGTT

AGCCTCAATGGCATCAGTTAC

Adcyap1: GAGAATCTGGGGGCAAGTCT

CACCAGCACCTGATCTGTCA

PENK: CCCAGGCGACATCAATTT

TCTCCCAGATTTTGAAAGAAGG

**Western Blot analysis**

Myc-tagged cDNA encoding NPAS4, BDNF, Pcsk1, Adcyap1, or PENK1 was transfected into 293T cells using Lipofectamine. Twenty four hours later cells were lysed in 2x Laemmli buffer and boiled for 5 minutes. Lysates were resolved by SDS-PAGE and immunoblotted with antibodies targeting Myc (1:1000, Abcam) or Actin (1:2500, Abcam). For expierments using neuronal lysates instead of heterologus cells, similar

procedures were used.

**Mouse cortical/hippocampal neuron culture**

E16.5 C57BL/6 embryonic mouse cortices were dissected and then dissociated for 10 min in 1× Hank's balanced salt solution (HBSS) containing 200ul papain (Roche) and 0.32 mg/mL L-cysteine (Sigma). Papain treatment was terminated by washing dissociated cells three times for 2 min each in dissociation medium consisting of 1× HBSS containing 10 mg/mL ovomucoid inhibitor (Worthington). Neurons were dissociated using a P1000 pipette tip with roughly 10 strokes. Neurons were plated immediately after dissociation

All plates were coated with 20 μg/mL poly-D-lysine (Sigma) and 4 μg/mL mouse laminin (Invitrogen) in water for at least 60 mins at 37C prior to plating neurons. Plates were briefly rinsed with 1x PBS (Invitrogen) before neurons were plated. Neurons were grown in neuronal medium consisting of Neurobasal medium containing B27 supplement (2%; Invitrogen), penicillin-streptomycin (50 g/mL penicillin and 50 U/mL streptomycin; Sigma) and glutaMAX (1 mM; Sigma).

Neurons were plated at a density of 25-30 million neurons per 15 cm plate or 1.25-1.5 million neurons per well on a 6-well plate. Neurons were cultured at 37 °C and 5% $CO_2$ for 7 days in vitro (DIV) unless explicitly stated otherwise. At 7 DIV, experimental assays commenced.

**Neuronal depolarization**

Neurons were depolarized by addition of depolarization buffer (170 mM KCl, 2 mM $CaCl_2$, 1 mM $MgCl_2$ and 10 mM HEPES pH 7.4) for the indicated duration. The final concentratoin of K+ was 55mM. Neurons were dissected as stated above and cultured for 7 days. On the $7^{th}$ day neurons were stimulated with depolarization buffer for the indicated time point.

**Preparation of neurons for ChIP**

5-80 million mouse cortical neurons were used for each ChIP and subsequence ChIP-seq library preparation. In general, histone and histone modification ChIP required 5-10 million cells whereas transcription factor ChIP requried 40-80 million neurons. Crosslinking was done with 1% formaldehyde for 10 minutes at room temperature. Crosslinking was quenched by adding 125mM glycine for 5 minutes at room temperature. Cells were then snap frozen and stored at -80C.

**ChIP-seq**

~1-10ng of ChIP DNA was used to generate Illumina compatible next generation sequencing libraries. All ChIP-seq library were generated using the Ovation ultra low library system (NuGEN). Samples were sequenced and demultiplexed on the Illumina NextSeq500. All ChIP-seq samples were sequenced to a depth of ~20-30 million reads per sample. Reads were aligned to the mouse genome (mm9) using BWA with default

settings. Peaks were called using Homer as per designer recommendations. Further analysis and display plots were done with custom written scripts in R.

**RNA-seq**

~1000ng of total RNA isolated with Qiazol (Qiagen) was used to generate Illumina compatible next generation sequencing libraries. All RNA-seq libraries were generated with NEBNext Ultra directional RNA library preparation kit (NEB) using manufacturer's recommendations. Samples were sequenced and demultiplexed on the Illumina NextSeq500. All RNA-seq samples were sequenced to a depth of ~40-80 million reads per sample. Reads were aligned to the mouse genome (mm9) using BWA with default settings. Transcript read densities were quantified using previous published custom written software (Kim et al., 2010). *Further* analysis and display plots were generated using custom written scripts in R.

**REFERENCES**

Adesnik, H., Li, G., During, M.J., Pleasure, S.J., and Nicoll, R.A. (2008). NMDA receptors inhibit synapse unsilencing during brain development. PNAS *105*, 5597-5602.

Atallah, B.V., Bruns, W., Carandini, M., and Scanziani, M. (2012). Parvalbumin-expressing interneurons linearly transform cortical responses to visual stimuli. Neuron *73*, 159-170.

Baldelli, P., Hernandez-Guijo, J.-M., Carabelli, V., and Carbone, E. (2005). Brain-Derived Neurotrophic Factor Enhances GABA Release Probability and Nonuniform Distribution of N- and P/Q-Type Channels on Release Sites of Hippocampal Inhibitory Synapses. J Neurosci *25*, 3358-3368.

Barco, A., Alarcon, J.M., and Kandel, E.R. (2002). Expression of constitutively active CREB protein facilitates the late phase of long-term potentiation by enhancing synaptic capture. Cell *108*, 689-703.

Blendy, J.A., Kaestner, K.H., Schmid, W., Gass, P., and Schutz, G. (1996). Targeting of the CREB gene leads to up-regulation of a novel CREB mRNA isoform. EMBO J *15*, 1098-1106.

Bourtchuladze, R., Frenguelli, B., Blendy, J., Cioffi, D., Schutz, G., and Silva, A.J.

(1994). Deficient long-term memory in mice with a targeted mutation of the cAMP-responsive element-binding protein. Cell *79*, 59-68.

Brigadski, T., Hartmann, M., and Lessmann, V. (2005). Differential vesicular targeting and time course of synaptic secretion of the mammalian neurotrophins. Journal of Neuroscience *25*, 7601-7614.

Buzsaki, G. (2002). Theta oscillations in the hippocampus. Neuron *33*, 325-340.

Buzsaki, G. (2005). Theta rhythm of navigation: link between path integration and landmark navigation, episodic and semantic memory. Hippocampus *15*, 827-840.

Castren, E., Safra, F., Thoenen, H., and Lindholm, D. (1996). Light regulates expression of brain-derived neurotrophic factor mRNA in rat visual cortex. PNAS *89*, 9444-9448.

Chen, J.L., Villa, K.L., Cha, J.W., So, P.T., Kubota, Y., and Nedivi, E. (2012). Clustered dynamics of inhibitory synapses and dendritic spines in the adult neocortex. Neuron *74*, 361-373.

Chiu, C.Q., Lur, G., Morse, T.M., N.T., C., Ellis-Davies, G.C., and Higley, M.J. (2013). Compartmentalization of GABAergic inhibition by dendritic spines. Science *340*, 759-762.

Cobb, S.R., Buhl, E.H., Halasy, K., Paulsen, O., and Somogyi, P. (1995). Synchronization of neuronal activity in hippocampus by individual GABAergic interneurons. Nature *378*, 75-78.

Cossart, R., Hirsch, J.C., Cannon, R.C., Dinoncourt, C., Wheal, H.V., Ben-Ari, Y., Esclapez, M., and Bernard, C. (2000). Distribution of spontaneous currents along the somato-dendritic axis of rat hippocampal CA1 pyramidal neurons. Neuroscience *99*, 593-603.

Danglot, L., Triller, A., and Marty, S. (2006). The development of hippocampal interneurons in rodents. Hippocampus *16*, 1032-1060.

Dash, P.K., Hochner, B., and Kandel, E.R. (1990). Injection of the cAMP-responsive element into the nucleus of Aplysia sensory neurons blocks long-term facilitation. Nature *345*, 718-721.

Dean, C., Liu, H., Staudt, T., Stahlberg, M.A., Vingill, S., Bückers, J., Kamin, D., Engelhardt, J., Jackson, M.B., Hell, S.W*., et al.* (2012). Distinct subsets of Syt-IV/BDNF vesicles are sorted to axons versus dendrites and recruited to synapses by activity. Journal of Neuroscience *32*, 5398-5413.

Edward S. Lein, A.H.C.J.S. (2000). Dynamic regulation of BDNF and NT-3 expression

during visual system development. The Journal of Comparative Neurology *420*, 1-18.

Falkenberg, T., Mohammed, A.K., Henriksson, B., Persson, H., Winblad, B., and Lindefors, N. (1992). Increased expression of brain-derived neurotrophic factor mRNA in rat hippocampus is associated with improved spatial memory and enriched environment. Neuroscience Letters *138*, 153-156.

Flavell, S.W., Cowan, C.W., Kim, T.K., Greer, P.L., Lin, Y., Paradis, S., Griffith, E.C., Hu, L.S., Chen, C., and Greenberg, M.E. (2006). Activity-dependent regulation of MEF2 transcription factors suppresses excitatory synapse number. Science *311*, 1008-1012.

Freund, T.F., and Buzsaki, G. (1996). Interneurons of the hippocampus. Hippocampus *6*, 347-470.

Fuentealba, P., Begum, R., Capogna, M., Jinno, S., Marton, L.F., Csicsvari, J., Thomson, A., Somogyi, P., and Klausberger, T. (2008). Ivy cells: a population of nitric-oxide-producing, slow-spiking GABAergic neurons and their involvement in hippocampal network activity. Neuron *57*, 917-929.

Gass, P., Wolfer, D.P., Balschun, D., Rudolph, D., Frey, U., Lipp, H.P., and Schütz, G. (1998). Deficits in memory tasks of mice with CREB mutations depend on gene dosage. Learning and Memory *5*, 274-288.

Ginty, D.D., Kornhauser, J.M., Thompson, M.A., Bading, H., Mayo, K.E., Takahashi, J.S., and Greenberg, M.E. (1993). Regulation of CREB phosphorylation in the suprachiasmatic nucleus by light and a circadian clock. Science *260*, 238-241.

Glickfeld, L.L., Atallah, B.V., and Scanziani, M. (2008). Complementary modulation of somatic inhibition by opioids and cannabinoids. J Neurosci *28*, 1824-1832.

Glickfeld, L.L., and Scanziani, M. (2006). Distinct timing in the activity of cannabinoid-sensitive and cannabinoid-insensitive basket cells. Nat Neurosci *9*, 807-815.

Greer, P.L., and Greenberg, M.E. (2008). From synapse to nucleus: calcium-dependent gene transcription in the control of synapse development and function. Neuron *59*, 846-860.

Han, J.H., Kushner, S.A., Yiu, A.P., Cole, C.J., Matynia, A., Brown, R.A., Neve, R.L., Guzowski, J.F., and Silva, A.J. (2007). Neuronal competition and selection during memory formation. Science *316*, 457-460.

Han, J.H., Kushner, S.A., Yiu, A.P., Hsiang, H.L., Buch, T., Waisman, A., Bontempi, B., Neve, R.L., Frankland, P.W., and Josselyn, S.A. (2009). Selective erasure of a fear memory. Science, 1492-1496.

Hubel, D.H., and Wiesel, T.N. (1963a). Receptive fields of cells in striate cortex of very young, visually inexperienced kittens. Journal of Neurophysiology, 994-1001.

Hubel, D.H., and Wiesel, T.N. (1963b). Shape and arrangement of columns in cat's striate cortex. Journal of Physiology *165*, 559-568.

Hummler, E., Cole, T.J., Blendy, J.A., Ganss, R., Aguzzi, A., Schmid, W., Beermann, F., and Schutz, G. (1994). Targeted mutation of the CREB gene: compensation within the CREB/ATF family of transcription factors. PNAS *91*, 5647-5641.

Kandel, E.R. (2001). The molecular biology of memory storage: a dialogue between genes and synapses. Science *294*, 1030-1038.

Kida, S., Josselyn, S.A., Ortiz, S.P.d., Kogan, J.H., Chevere, I., Masushige, S., and Silva, A.J. (2002). CREB required for the stability of new and reactivated fear memories. Nature Neuroscience *5*, 348-355.

Kim, J., Kwon, J.T., Kim, H.S., Josselyn, S.A., and Han, J.H. (2014). Memory recall and modifications by activating neurons with elevated CREB. Nature Neuroscience *17*, 65-72.

Kim, T.K., Hemberg, M., Gray, J.M., Costa, A.M., Bear, D.M., Wu, J., Harmin, D.A.,

Laptewicz, M., Barbara-Haley, K., Kuersten, S.*, et al.* (2010). Widespread transcription at neuronal activity-regulated enhancers. Nature *465*, 182-187.

Klausberger, T. (2009). GABAergic interneurons targeting dendrites of pyramidal cells in the CA1 area of the hippocampus. Eur J Neurosci *30*, 947-957.

Klausberger, T., Magill, P.J., Marton, L.F., Roberts, J.D., Cobden, P.M., Buzsaki, G., and Somogyi, P. (2003). Brain-state- and cell-type-specific firing of hippocampal interneurons in vivo. Nature *421*, 844-848.

Klausberger, T., Marton, L.F., O'Neill, J., Huck, J.H., Dalezios, Y., Fuentealba, P., Suen, W.Y., Papp, E., Kaneko, T., Watanabe, M.*, et al.* (2005). Complementary roles of cholecystokinin- and parvalbumin-expressing GABAergic neurons in hippocampal network oscillations. J Neurosci *25*, 9782-9793.

Kogan, J.H., Frankland, P.W., Blendy, J.A., Coblentz, J., Marowitz, Z., Schütz, G., and Silva, A.J. (1997). Spaced training induces normal long-term memory in CREB mutant mice. Current Biology *7*, 1-11.

Kohara, K., Yasuda, H., Huang, Y., Adachi, N., Sohya, K., and Tsumoto, T. (2007). A Local Reduction in Cortical GABAergic Synapses after a Loss of Endogenous Brain-Derived Neurotrophic Factor, as Revealed by Single-Cell Gene Knock-Out Method. J

Neurosci *27*, 7234-7244.

Larkum, M.E., Zhu, J.J., and Sakmann, B. (1999). A new cellular mechanism for coupling inputs arriving at different cortical layers. Nature *398*, 338-341.

Lee, S.H., Kwan, A.C., Zhang, S., Phoumthipphavong, V., Flannery, J.G., Masmanidis, S.C., Taniguchi, H., Huang, Z.J., Zhang, F., Boyden, E.S.*, et al.* (2012). Activation of specific interneurons improves V1 feature selectivity and visual perception. Nature *488*, 379-383.

Lin, Y., Bloodgood, B.L., Hauser, J.L., Lapan, A.D., Koon, A.C., Kim, T.K., Hu, L.S., Malik, A.N., and Greenberg, M.E. (2008). Activity-dependent regulation of inhibitory synapse development by Npas4. Nature *455*, 1198-1204.

Liu, G. (2004). Local structural balance and functional interaction of excitatory and inhibitory synapses in hippocampal dendrites. Nat Neurosci *7*, 373-379.

Lonze, B.E., and Ginty, D.D. (2002). Function and regulation of CREB family transcription factors in the nervous system. Neuron *35*, 605-623.

Lonze, B.E., Riccio, A., Cohen, S., and Ginty, D.D. (2002). Apoptosis, axonal growth defects, and degeneration of peripheral neurons in mice lacking CREB. Neuron *34*, 371-

385.

Lovett-Barron, M., Turi, G.F., Kaifosh, P., Lee, P.H., Bolze, F., Sun, X.H., Nicoud, J.F., Zemelman, B.V., Sternson, S.M., and Losonczy, A. (2012). Regulation of neuronal input transformations by tunable dendritic inhibition. Nature Neuroscience, 423-430.

Lu, W., Shi, Y., Jackson, A.C., Bjorgan, K., During, M.J., Sprengel, R., Seeburg, P.H., and Nicoll, R.A. (2009). Subunit composition of synaptic AMPA receptors revealed by a single-cell genetic approach. Neuron *62*, 254-268.

Malinow, R. (2003). AMPA receptor trafficking and long-term potentiation. Philos Trans R Soc Lond B Biol Sci *358*, 707-714.

Marty, S., Wehrlé, R., and Sotelo, C. (2000). Neuronal activity and brain-derived neurotrophic factor regulate the density of inhibitory synapses in organotypic slice cultures of postnatal hippocampus. Journal of Neuroscience *20*, 8087-8095.

Miles, R., and Poncer, J.C. (1996). Paired recordings from neurones. Curr Opin Neurobiol *6*, 387-394.

Miles, R., Toth, K., Gulyas, A.I., Hajos, N., and Freund, T.F. (1996). Differences between somatic and dendritic inhibition in the hippocampus. Neuron *16*, 815-823.

Montarolo, P.G., Goelet, P., Castellucci, V.F., Morgan, J., Kandel, E.R., and Schacher, S. (1986). A critical period for macromolecular synthesis in long-term heterosynaptic facilitation in Aplysia. Science *234*, 1249-1254.

Pattabiraman, P.P., Tropea, D., Chiaruttini, C., Tongiorgi, E., Cattaneo, A., and Domenici, L. (2005). Neuronal activity regulates the developmental expression and subcellular localization of cortical BDNF mRNA isoforms in vivo. Molecular and Cellular Neuroscience *28*, 556-570.

Pittenger, C., Huang, Y.Y., Paletzki, R.F., Bourtchouladze, R., Scanlin, H., Vronskaya, S., and Kandel, E.R. (2002). Reversible inhibition of CREB/ATF transcription factors in region CA1 of the dorsal hippocampus disrupts hippocampus-dependent spatial memory. Neuron *34*, 447-462.

Ploski, J.E., Monsey, M.S., Nguyen, T., DiLeone, R.J., and Schafe, G.E. (2011). The neuronal PAS domain protein 4 (Npas4) is required for new and reactivated fear memories. PLoS One *6*, e23760.

Pouille, F., Marin-Burgin, A., Adesnik, H., Atallah, B.V., and Scanziani, M. (2009). Input normalization by global feedforward inhibition expands cortical dynamic range. Nature Neuroscience *12*, 1577-1585.

Pouille, F., and Scanziani, M. (2001). Enforcement of temporal fidelity in pyramidal cells by somatic feed-forward inhibition. Science *293*, 1159-1163.

Pouille, F., and Scanziani, M. (2004). Routing of spike series by dynamic circuits in the hippocampus. Nature *429*, 717-723.

Ramamoorthi, K., Fropf, R., Belfort, G.M., Fitzmaurice, H.L., McKinney, R.M., Neve, R.L., Otto, T., and Lin, Y. (2011). Npas4 regulates a transcriptional program in CA3 required for contextual memory formation. Science *334*, 1669-1675.

Riccio, A., Ahn, S., Davenport, C.M., Blendy, J.A., and Ginty, D.D. (1999). Mediation by a CREB family transcription factor of NGF-dependent survival of sympathetic neurons. Science *286*, 2358-2361.

Rocamora, N., Welker, E., Pascual, M., and Soriano, E. (1996). Upregulation of BDNF mRNA expression in the barrel cortex of adult mice after sensory stimulation. Journal of Neuroscience *16*, 4411-4419.

Royer, S., Zemelman, B.V., Barbic, M., Losonczy, A., Buzsaki, G., and Magee, J.C. (2010). Multi-array silicon probes with integrated optical fibers: light-assisted perturbation and recording of local neural circuits in the behaving animal. Eur J Neurosci *31*, 2279-2291.

T.F. Freund, G.B. (1996). Interneurons of the hippocampus. Hippocampus *6*, 347-470.

Turner, D., and Schwartzkroin, P. (1983). Electrical characteristics of dendrites and dendritic spines in intracellularly stained CA3 and dentate hippocampal neurons. J Neurosci *3*, 2381-2394.

Turrigiano, G.G., Leslie, K.R., Desai, N.S., Rutherford, L.C., and Nelson, S.B. (1998). Activity-dependent scaling of quantal amplitude in neocortical neurons. Nature *391*, 892-896.

Versendaal, D.v., Rajendran, R., Saiepour, M.H., Klooster, J., Smit-Rigter, L., Sommeijer, J.P., Zeeuw, C.I.D., Hofer, S.B., Heimel, J.A., and Levelt, C.N. (2012). Elimination of inhibitory synapses is a major component of adult ocular dominance plasticity. Neuron *74*, 374-383.

Waddell, S., and Quinn, W.G. (2001). What can we teach Drosophila? What can they teach us? Trends Genetic *12*, 719-726.

West, A.E., Griffith, E.C., and Greenberg, M.E. (2002). Regulation of transcription factors by neuronal activity. Nat Rev Neurosci *3*, 921-931.

Wiesel, T.N., and Hubel, D.H. (1963). Effects of visual deprivation on morphology and physiology of cells in the cat's lateral geniculate body. Journal of Neurophysiology, 978-

993.

Wilson, N.R., Runyan, C.A., Wang, F.L., and Sur, M. (2012). Division and subtraction by distinct cortical inhibitory networks in vivo. Nature *488*, 343-348.